Remodeling of the secretory pathway is coordinated with *de novo* membrane formation in budding yeast gametogenesis

Yasuyuki Suda[1, 2]*, Hiroyuki Tachikawa[3], Tomomi Suda[1], Kazuo Kurokawa[2], Akihiko Nakano[2], and Kenji Irie[1]

[1] Department of Molecular Cell Biology, Faculty of Medicine, University of Tsukuba, Tsukuba, Ibaraki, Japan.

[2] Live Cell Super-Resolution Imaging Research Team, RIKEN Center for Advanced Photonics, Wako, Saitama, Japan.

[3] Department of Applied Biological Chemistry, Graduate School of Agriculture and Life Sciences, The University of Tokyo, Tokyo, Japan.

*Corresponding Author: Yasuyuki Suda
Laboratory of Molecular Cell Biology,
Faculty of Medicine, University of Tsukuba,
1-1-1 Tennodai, Tsukuba, Ibaraki 305-8575, Japan.
TEL: +81-29-853-3066; FAX: +81-29-853-3066
E-mail: ysuda@md.tsukuba.ac.jp

Abstract

Gametogenesis in budding yeast involves large-scale rearrangement of membrane traffic to allow *de novo* formation of a membrane, called the prospore membrane (PSM). However, the mechanism underlying this event is not fully elucidated. Here, we show that the number of endoplasmic reticulum exit sites (ERES) per cell fluctuates and switches from decreasing to increasing upon the onset of PSM formation. Reduction in ERES number is accompanied by a transient stall in membrane traffic, resulting in loss of the preexisting Golgi apparatus from the cell, as well as local ERES regeneration, leading to Golgi reassembly in nascent spores. We have revealed that protein phosphatase-1 (PP-1) and its development-specific subunit, Gip1, promote ERES regeneration through Sec16 foci formation. Furthermore, a mutant with impaired ERES formation showed defects in PSM growth and spore formation. Thus, ERES regeneration in nascent spores facilitates the segregation of membrane traffic organelles, leading to PSM growth.

Key words: sporulation, meiosis, membrane traffic, Endoplasmic reticulum, Golgi apparatus, ER exit sites, Saccharomyces cerevisiae, Sec16, COPII

Introduction

Gametogenesis of budding yeast, a developmental process consisting of meiosis and spore formation, in which chromosomes stored within the nucleus undergo a single round of replication followed by two successive rounds of segregation to produce haploid gametes. In meiosis II, a newly generated membrane, the prospore membrane (PSM), is formed at the cytoplasmic surface of the spindle pole body (SPB) embedded in the nuclear membrane, and the haploid set of chromosomes in the nucleus is engulfed by the growing PSM, along with organelles and cytosol[1]. This process is triggered by starvation and accompanied by a massive remodeling in the mother cell and is carried out through the strict control of transcription and translation, which also depends on membrane traffic[1,2]. Hence, a sporulating cell regulates the number of spores by producing the PSM only at modified SPBs in response to the available nutrients, resulting in the formation of fewer than four spores per cell[3,4].

In mitotic cell growth, both secretory cargo molecules and lipids synthesized in the endoplasmic reticulum (ER) are first transported to the Golgi apparatus then sorted to their final destinations, post-Golgi compartments and the extracellular space. The itinerary of this default secretory pathway is dramatically altered during meiosis, and its destination is changed to the PSM[5]. In this case, the formation of the PSM is initiated by converting the molecular mechanisms of post-Golgi vesicle fusion with the plasma membrane in mitotic cells, and limiting the location of vesicle fusion to the cytoplasmic surface of the SPB[6]. The mother cell requires a large supply of lipids to generate from scratch the large membrane structures that later become the gamete's plasma membrane. To accomplish this, not only the conversion of membrane traffic but also lipid transport by Vps13, a newly identified lipid transporter, and its adaptor complex, are required[7–11]. The Vps13 complex is assumed to transport lipids directly from the ER to the PSM through its hydrophobic tunnel-like structure[7,12]. Although various studies have shed light on the mechanisms of nascent PSM formation, the integrated regulation of membrane traffic throughout the cell during meiotic progression remains unclear.

Transport of cargo proteins from the ER is mediated by the COPII transport carrier that is formed at specialized ER subdomains called ER exit sites (ERES)[13]. The COPII carrier consists of inner coat Sec23-Sec24 and outer coat Sec13-Sec31 complexes that are recruited to the membrane by the active Sar1-GTPase[14]. ERES are preferentially formed at the high-curvature domain of the ER that is composed of fenestrated sheets and tubules[15]. Sec16 is a large peripheral membrane protein and a key molecule for ERES organization, since its dysfunction causes failure of COPII-mediated transport as well as ERES formation[16,17]. The potential function of Sec16 in ERES organization is widely conserved

74 throughout eukaryotes, but its regulation differs among organisms[18]. In mammals, during
75 mitosis, the ERES collapse and the Golgi fragment disperses into the cytoplasm, thereby
76 the secretory pathway is transiently attenuated[19,20]. In *Drosophila melanogaster*, upon
77 starvation, Sec16 is released from the ER membrane and sequestered in a
78 phase-separated granule with several COPII-forming factors[21]. This sequestration is
79 bidirectional and is assumed to function as a reservoir to initiate COPII formation quickly
80 after recovery from starvation. Mammalian cell division and the starvation response of flies
81 are processes that involve large-scale remodeling, in which cells employ integrated
82 regulation of membrane traffic via its starting point, the ERES. Gametogenesis in budding
83 yeast also involves cellular remodeling, but it is not well understood whether ERES
84 formation is similarly regulated.

85 We previously showed that the cortical ER, a subset of the ER closely associated
86 with the plasma membrane, is reorganized upon PSM formation and that the PSM acts as a
87 border to keep the Golgi apparatus inside[22]. More recently, the molecular mechanisms
88 responsible for the morphology of the ER during meiosis and for the distribution of the
89 mitochondria have also been elucidated[23,24]. Although these organellar remodeling
90 processes are shown to be a system to exclude unnecessary organelles rather than an
91 active transport machinery toward the gametes, they are crucial to the cell, as it is inherently
92 linked to cell rejuvenation by eliminating age-related factors from the gametes[2,25]. In this
93 case, the PSM provides a barrier between age-related factors such as damaged organelles
94 and those including chromosomes to be inherited by the next generation. Thus the progeny
95 become protected by the robust spore wall formed in the lumen of PSMs, while the
96 remaining age-related factors are degraded either by autophagy and subsequent vacuolar
97 rupture[26].

98 In this study, we revealed the dynamics of ERES during gametogenesis and its
99 involvement in PSM formation; ERES formation is transiently inactivated during meiosis,
100 while ERES regeneration is locally activated in the region surrounded by the PSM in meiosis
101 II to extend the PSM. Analysis of mutants defective in PSM formation revealed that Gip1, a
102 meiosis-specific targeting subunit of PP1[27,28], functions in ERES remodeling, and whose
103 direct contribution to PSM formation was previously unknown. PP1-dependent ERES
104 remodeling occurs through Sec16, and the analysis of factors involved in COPII-carrier
105 formation suggests that the reorganization of membrane traffic in presumptive spores is the
106 system responsible for the segregation of membrane traffic into gametes, and that lipid
107 supply through the secretory pathway contributes to PSM growth. Overall, our study
108 suggests that developmental regulation of membrane traffic coordinates *de novo* membrane
109 formation and organellar segregation to the progeny.

Results

ERES numbers fluctuate in meiosis.

Meiotic development includes the faithful inheritance of essential organelles such as the nucleus, mitochondria, and ER for the generation of spore gametes. To characterize morphologies of the organelles for membrane traffic in detail upon meiotic development, time-course observation of the ER was performed in cells expressing the transmembrane domain of ER-localized tethering protein, Scs2, fused with mNeonGreen (mNG-Scs2TM) and chromatin (Htb2-mCherry) (Fig. 1A). In premeiotic cells, reticular cortical ER expanded underneath the plasma membrane and was retained as in vegetatively growing cells (Fig. 1A. 0-3 hrs). Detachment of cortical ER from the plasma membrane and the expansion of cytoplasmic ER were observed before the first meiotic division (Fig. 1A. 4 hr), then they were subsequently lost as meiosis progressed, presumably being absorbed into the nuclear ER (Fig. 1A. 5 hr-). In metaphase II to anaphase II cells, ER signals were detected in association with dividing nuclei (Fig. 1A. 6-9 hrs), similar to that observed previously[22]. Subsequently, regeneration of the cortical ER underneath the spore plasma membrane was seen after completion of spore maturation (Fig. 1A. 10 hr), consistent with the prior data[23].

ERES are sites for the assembly of COPII transport carriers and are formed preferentially at the high-curvature domain of the ER[15]. Observation of ERES, visualized by Sec13-GFP, in pre-meiotic cells showed numerous spots in the peripheral region of the cell. In contrast, as meiosis progresses, cells showed the disappearance of a cortically localized portion of ERES; instead, they accumulate in the cytoplasm (Fig. 1B). To analyze ERES dynamics in meiotic development, time-course observation of ERES was also performed with chromatin marked by Htb2-mCherry (Fig. 1C). Numerous punctate structures of ERES in premeiotic cells were similarly observed as in mitotic cells, but their number gradually decreased and then increased after metaphase II (Fig. 1D). Although the number of ERES fluctuated gradually during meiotic progression, average signal intensities for Sec13-GFP were relatively stable (Fig. S1A, S1B). We reasoned that the observed change in the number of ERES could correspond to the activity of COPII generation. In the fruit fly, *D. melanogaster*, amino acid starvation leads to the coalescence of Sec16, the scaffold protein for the assembly of COPII transport carriers, into large membrane-less organelles called sec bodies, which are thought to act as a reservoir for ERES in harsh conditions[21]. In our condition for budding yeast meiosis, Sec16-GFP was similarly distributed and colocalized with Sec13-mCherry (Fig. S1C, S1D). Analyzing Sec13-GFP dynamics by fluorescence recovery after photobleaching (FRAP), we showed that Sec13-GFP molecules exchange rapidly between ERES and the cytoplasm in vegetatively growing cells. The half-time to recovery was 4.6 seconds (+/- 2.4 seconds). By contrast, in cells undergoing meiosis, the

146 half-time to recovery for meiosis I and II was 18.8 seconds (+/- 16.9 seconds) and 26.5
147 seconds (+/- 21.6 seconds), respectively (Fig. S1E and S1F). These data indicate that the
148 activity of ERES persists, but its dynamics specifically slowed down in the progression of
149 meiosis.
150
151 **ERES forms *de novo* in the spore cytoplasm.**
152 In anaphase II cells, ERES always localize in association with dividing
153 chromosomes and were considered to be segregated to gametes. Indeed, ERES were
154 precisely segregated into presumptive spores (Fig. 1C). We next investigated the proper
155 timing of ERES segregation into nascent spores. The PSM is formed by the coalescence of
156 post-Golgi vesicles at the cytoplasmic face of SPBs[1]. Based on time-course observation of
157 PSM perimeters, PSM growth was categorized into the initial fusion process, horseshoe,
158 elongation, and mature stages[10], and ERES segregation was found in cells with the
159 horseshoe stage (Fig. 1C). To further characterize the segregation of ERES during PSM
160 formation, we then performed 3D live-cell imaging of ERES and PSM dynamics by
161 super-resolution confocal live imaging microscopy (SCLIM)[29,30]. ERES first appeared inside
162 the PSM at the stage (~12 min) in which the PSM showed horseshoe-like morphology, then
163 ERES proliferated inside PSMs during the elongation stage until the completion of PSM
164 maturation (Fig. 1E and Movie S1). Taken together, these data reveal that the collapse of
165 ERES leads to the decrease of their number in the cell during meiotic progression until the
166 onset of PSM formation, then they are formed *de novo* and proliferate in the cytoplasm of
167 nascent spores.
168
169 **Change in ERES number coincides with the Golgi disappearance and reappearance.**
170 In yeast, the Golgi can form *de novo*, as COPII vesicles arising from ERES fuse to
171 form a post-ER compartment and then presumably mature into *cis*-cisterna of the Golgi[13,31].
172 We have previously shown that the nascent PSM functions as a diffusion barrier for the
173 Golgi[22], however, detailed dynamics of the ER-Golgi unit during meiosis have not been
174 examined. To this end, we investigated whether the collapse and regeneration of the Golgi
175 in cells are also observed during meiotic progression and PSM formation. To observe the
176 Golgi apparatus, we chose the fluorescently tagged Golgi-resident proteins, Mnn9-sfGFP, a
177 *cis*-Golgi resident mannosyltransferase, Sys1-Envy, a receptor for Arl3 GTPase residing in
178 *trans*-Golgi, and *trans*-Golgi network (TGN) marker, Sec7-Envy[32,33] (Fig. 2). Although
179 numerous spots for these markers were seen in vegetative and pre-meiotic cells (Fig. 2,
180 Initial-stages), signals at the Golgi were not detected in a certain population of the cells in
181 the early process of PSM formation (Fig. 2A, 2B, horseshoe-stages). Note that weak signals

182 for Mnn9-sfGFP at the ER and Sys1-Envy at the vacuole were observed in these cells. As
183 the PSM elongates, however, the presumptive spores completely acquired dot-like signals
184 for these marker proteins (Fig. 2A, 2B, arrowheads in elongation-stages). These
185 observations could reflect both disassembly and regeneration of the Golgi during the
186 formation of PSMs, which might be based on the change of ERES number in meiosis. A
187 similar tendency was also observed for Sec7-Envy, a TGN-localized marker, which
188 appeared much earlier in PSM growth (Fig. 2C). These findings indicate that the decrease in
189 the number of Golgi foci corresponds to the decrease in ERES number, and they
190 reassemble within the spore cytoplasm possibly from the fusion of COPII vesicles arising
191 from ERES.
192
193 **Determinants of ER shape are important for change in ERES numbers.**
194 The site of ERES formation is restricted to the high-curvature region of the ER[15].
195 As reticulons and DP1/Yop1 are factors stabilizing the network-like morphology of the ER[34],
196 ERES accumulate at the edge of the expanded sheet of the ER in *rtn1*Δ *rtn2*Δ *yop1*Δ cells[15].
197 In meiosis, reticulon-mediated ER curvature has been reported to lead directly or indirectly
198 to the cortical detachment and cabling of the ER[23]. To test whether the changes in ERES
199 numbers are also affected in this situation, we analyzed the morphology of the ER and the
200 distributions of ERES numbers in *rtn1*Δ *rtn2*Δ *yop1*Δ cells. Consistent with the previous
201 observation[23], there was no expansion of the cytoplasmic ER or absorption into the nuclear
202 ER, rather smooth, sheet-like structures were retained near the cortical region of the cell
203 (Fig. 3A, 3B). Thus, the cytoplasmic expansion is the result of the detachment of cortical ER.
204 The number of ERES was not decreased but rather persisted in metaphase II (Fig. 3C),
205 corresponding to the observed defect in morphological change of the ER in *rtn1*Δ *rtn2*Δ
206 *yop1*Δ cells. These results suggest that the number and distribution of ERES are linked, at
207 least in part, to the morphological change of the ER in meiotic development.
208
209 **ERES regeneration within spores requires a meiosis-specific PP1 subunit.**
210 To clarify the molecular basis for ERES regeneration within the spore cytoplasm,
211 we carried out visual inspection among the mutants displaying defects in the morphological
212 development of the PSM, including *gip1*Δ, *vps13*Δ, *spo71*Δ, *spo73*Δ, *sma2*Δ, *spo1*Δ,
213 *spo19*Δ[10,28,35–37]. In this analysis, *gip1*Δ showed obvious ERES regeneration defect; no
214 ERES foci were observed inside the PSM (Fig. 4A, upper panels, and 4B). Gip1 is a
215 sporulation-specific targeting subunit for Glc7, the sole catalytic subunit of PP1 in budding
216 yeast, and *gip1*Δ showed multiple defects in spore development such as septin organization,
217 PSM growth, and spore wall formation[27,28]. PSM extension is facilitated independently by

218 unknown functions of PP1-Gip1 and Vps13-mediated lipid transport[27]. Although a similar
219 PSM growth defect has been shown in mutants for Vps13 and its adaptor complex
220 Spo71-Spo73[10], ERES distributed inside the PSM in these mutant cells (Fig. 4A, lower
221 panels, and 4B). Time-course analyses of the numbers of ERES distributions in *gip1*Δ and
222 *vps13*Δ mutants were indistinguishable from that in wild-type cells (Fig. 4C and Fig. 1C, 1D).
223 In *gip1*Δ cells, the initial process of PSM formation was normal, but the elongation was
224 defective, stopping at the horseshoe-stage (PSM perimeter of almost 6 μm) (Fig. 4D, *gip1*Δ).
225 Whereas ERES regeneration was observed in most of the wild-type cells with a PSM
226 perimeter of at least 2 μm (Fig. 4E, wt), the *gip1*Δ PSM failed to contain ERES, even in cells
227 with PSM lengths greater than 2 μm perimeters (Fig. 4E, *gip1*Δ). To assess how the
228 observed defect in ERES regeneration in *gip1*Δ, we conducted 3D live-cell imaging using
229 SCLIM. Observation of Sec13-GFP in *gip1*Δ cells showed no ERES signals accumulate
230 within the spore cytoplasm along with the defect in PSM elongation (Fig. 5A and Movie S2).
231 Quantification of the signal intensity ratio of Sec13-GFP between inside the PSM and the
232 entire cell, clearly showed that the *de novo* formation of ERES within the PSM in wild-type
233 cells, that was not observed in *gip1*Δ cells (Fig. 5B). No characteristic defect in the ER
234 morphological change was found in the *gip1*Δ mutant during meiosis (Fig. 5C). In *gip1*Δ cells,
235 regeneration of the Golgi was completely abolished in all PSMs formed (Fig. 5D).
236 Collectively, we propose that Gip1 is required for ERES regeneration in nascent spores to
237 establish membrane traffic, leading to PSM elongation.
238 To determine whether the observed ERES regeneration defect in *gip1*Δ cells is
239 caused by a failure to properly localize Glc7 or a specific function of Gip1 itself, we next
240 examined the localization of GFP-Glc7 in *gip1*Δ cells, then ERES regeneration in the
241 *glc7-136* mutant, in which the Glc7 protein is defective in association with Gip1[38]. In
242 wild-type cells, GFP-Glc7 was first seen as dots inside the small circular PSM, which may
243 reflect transient SPB localization. Then GFP-Glc7 showed septin-like parallel bars along
244 with the growing PSM, and finally appeared in the nucleus after PSM maturation (Fig. 6A).
245 These localization patterns of GFP-Glc7 are consistent with the dynamic localization of Gip1
246 during PSM formation, which we have shown previously[27]. In *gip1*Δ cells, SPB-localization
247 of GFP-Glc7 was normal, but the subsequent characteristic localizations along the PSM and
248 septin was not observed (Fig. 6B). Moreover, ERES regeneration defect was similarly
249 observed in the *glc7-136* mutant allele (Fig. 6C). Previously, we mapped the
250 septin-localization domain in Gip1, and the deletion of this domain (Gip1-Δsep) resulted in
251 protein localization at the PSM instead of proper localization with septin[27], but neither PSM
252 growth nor sporulation defects were seen under this condition. Consistently, Gip1-Δsep was
253 able to suppress completely the ERES regeneration defect in *gip1*Δ cells, as the wild-type

254 version of Gip1 did (Fig. S2). Thus, the defect in ERES regeneration in *gip1*Δ can be the
255 consequence of the failure to recruit Glc7 to the PSM during PSM formation.
256 The next question is how the PP1-Gip1 signal is transmitted to ERES formation?
257 We hypothesize that the factor organizing ERES is the transducer of PP1-Gip1 during
258 sporulation and Sec16 is a candidate. In wild-type cells, Sec16-2xyEGFP foci were
259 distributed along the nucleus, which underwent alterations in miotic progression, and were
260 precisely segregated into the nascent spore cytoplasm, consistent with the observation of
261 ERES visualized with Sec13-GFP (Fig. 6D, 6E). In *gip1*Δ cells, we found that
262 Sec16-2xyEGFP was unable to form foci upon transition from the initial to horseshoe-stage
263 of PSM formation (Fig. 6F). Thus, whether directly or indirectly, PP1-Gip1 transduces
264 signals toward ERES regeneration via development of Sec16 foci during PSM formation.
265
266 **Defect in ERES formation also affects PSM extension.**
267 Since PSMs are formed by the fusion of post-Golgi vesicles[1], analysis of *SEC*
268 genes for their effects on PSM formation has been limited to late-acting *SEC* genes[6]. Thus,
269 we investigated the effect of components required/important for COPII carrier and ERES
270 formation on sporulation. Most of these components are essential for growth, but deletions
271 of some relatively minor components for ERES and COPII formation are viable. One of
272 these components, Sed4 is a non-essential paralog of Sec12, the ER-resident
273 transmembrane guanine-nucleotide-exchange-factor (GEF) for Sar1 GTPase, which has no
274 catalytic activity toward Sar1, but is proposed to stimulate Sar1 activity[39–41]. We found that a
275 single deletion mutant for *SED4* has defect in sporulation (Fig. 7A). Consistent with the
276 proposed mitotic localization of Sec12 and Sed4, at the entire ER and dot-like signals on the
277 ER, respectively[42], similar localizations of GFP-Sec12 and GFP-Sed4 were observed during
278 sporulation (Fig. 7B). When we observed the Sec13-GFP and mCh-Spo20$^{51-91}$ in *sed4*Δ, a
279 significant fraction of the *sed4*Δ cells showed defective ERES segregation and unequal,
280 aberrant PSM extension (Fig. 7C, 7D). These defects were suppressed by introducing either
281 full-length Sed4 or Sed4 lacking the luminal domain, which is dispensable for its function[39]
282 (Fig. 7C). Live-cell imaging of ERES and the PSM by SCLIM showed that, in *sed4*Δ cells,
283 ERES formation was normal within the PSM that showed a relatively normal extension rate,
284 but was defective within PSMs defective in extension (Fig. 7E, 7F, and Movie S3). These
285 results again confirmed that the *de novo* formation of ERES is indeed required for the
286 subsequent extension of PSMs.

287 **Discussion**

288 We investigated the dynamics of secretory pathway organelles in budding yeast
289 during the formation of *de novo* membranes in meiosis. In this analysis, we found that the
290 number of ERES, the starting point of membrane traffic, per cell decreased, and then
291 increased after anaphase II. The increase in ERES number was attributed to their
292 regeneration, which was restricted within the cytoplasmic space surrounded by the newly
293 formed PSM. Furthermore, we showed that ERES regeneration could be mediated through
294 Sec16 and is triggered by PP1-Gip1, which is specifically targeted to the inner surface of
295 PSMs during meiosis. A mutant defective in both COPII carrier and ERES formation showed
296 the PSM growth defect that is reminiscent to the defect in *gip1*Δ cells, suggesting a possible
297 link between these pathways. In sum, our results revealed that developmentally regulated
298 ERES regeneration is essential for PSM growth by mediating the segregation of organelles
299 that constitute membrane traffic, including the Golgi, which presumably supplies membrane
300 lipids to PSMs through the secretory pathway (Fig. 8). This process may also contribute to
301 the renewal of secretory pathway organelles that have been damaged through aging,
302 leading to maintenance of proteostasis.

303

304 **Meiosis-specific ERES regeneration leads to both PSM formation and segregation of**
305 **the secretory pathway organelles into gametes**

306 In mitosis, the number of ERES fluctuates, according to the processes of assembly
307 and disassembly, fusion and fission[15–17,43]. In the present study, we have observed that the
308 ERES numbers gradually decrease as meiosis progresses, and increase after the onset of
309 PSM formation due to local regeneration in the nascent spore cytoplasm. The ERES
310 dynamics and *gip1*Δ phenotype for local ERES regeneration led us to propose that there is a
311 signal that directly/indirectly represses ERES formation through Sec16 in the early stages of
312 meiosis. At the onset of PSM formation, however, ERES formation is de-repressed in a
313 Gip1-dependent manner. Although numerous phosphorylation sites have been found in
314 Sec16, their specific roles remain unclear[44]. Importantly, since the mutations in these
315 phosphorylated amino acids did not show any defects, either in meiotic progression or PSM
316 formation (data not shown), specific regulation could exist in meiosis. Candidate signaling
317 pathways to inhibit ERES formation include regulators that act early in meiosis, such as
318 Cdc5 and Hrr25[45,46]. In mammalian cells, secretion mediated by membrane traffic pauses
319 during mitosis[47]. This phenomenon is due to the disruption of the early secretory pathway
320 that is composed of ERES and the Golgi, and some parts of the mechanism have been
321 shown recently[20]. ERES formation in mammals is determined by the interaction between
322 Sec16 and TANGO1, and the affinity of TANGO1 for Sec16 is regulated by phosphorylation

323 in a cell cycle-dependent manner. The phosphorylation status of TANGO1 is in equilibrium
324 through the action of CK1 and PP1, but PP1 activity is specifically decreased during mitosis,
325 leading to the dissociation of Sec16 from the ER and ERES disassembly[19]. Although
326 TANGO1 is absent in budding yeast, development-specific regulation of Sec16 recruitment
327 could exist. We found that the mutant of Sed4, a regulator of the Sar1 GTPase cycle and
328 Sec16 localization to ERES[39,48], partially phenocopied the *gip1*Δ phenotype, suggesting a
329 possible involvement of these factors in the ERES formation in meiosis.
330 Our previous analysis of organellar segregation in sporulation is inconclusive as to
331 whether the Golgi segregation into spores is mediated through the active transport or PSMs
332 act as a diffusion barrier for the Golgi[22]. In the present study, we showed that local
333 regeneration of ERES and the Golgi occurs specifically in the spore cytoplasm in wild-type
334 cells, but neither was observed in *gip1*Δ cells. Thus, the Golgi apparatus is once dissipated
335 from the cell and reassembled specifically within the nascent spores during meiosis, and
336 this phenomenon is equivalent to the mitotic disassembly and reassembly of the Golgi in
337 mammalian cells. How the Golgi apparatus is formed and maintained in cells remains
338 elusive. To clarify such questions, live cell observations of the Golgi regeneration were
339 conducted in plant cells using a drug that induces Golgi disassembly followed by its
340 washout[49,50]. Results from the study showed that the Golgi enzymes are absorbed into the
341 ER upon disassembly and return to the Golgi through ERES when the Golgi is reassembled
342 by drug washout. Moreover, a subset of the Golgi-resident proteins underwent nucleation
343 near ERES as a template for Golgi regeneration occurring upon drug removal, leading the
344 authors to conclude that it served as the scaffold for Golgi regeneration, called Golgi entry
345 core compartment (GECCO)[49,51]. A similar scaffold for Golgi regeneration could be also
346 present in budding yeast and segregated first in the vicinity of SPBs during PSM formation.
347 The molecular mechanism underlying this phenomenon in meiosis is clearly regulated by
348 PP1-Gip1, and similar mechanisms might be involved in Golgi regeneration in mitosis.
349 PP1-Gip1 is also essential for the formation of the septin higher-order structure that
350 forms beneath PSMs, where it localizes to this formed structure[28]. We previously identified a
351 septin localization domain of Gip1, and showed that the Gip1 mutant that lacks this domain
352 (Gip1Δsep) can also trigger ERES formation and PSM formation[27]. This result is in
353 agreement with our previous report, in which the localization of PP1-Gip1 around PSMs is
354 sufficient for its function[27]. The observed sporulation defects in *gip1*Δ cells can be explained
355 by Gip1's function as a trigger for membrane traffic remodeling and its contribution to PSM
356 formation.
357
358 **Nutrient starvation-triggered meiotic remodeling in yeast**

359 In flies, and more recently in mammals, nutrient starvation is shown to result in the
360 formation of a membrane-less structures of Sec16, called Sec bodies, by liquid-liquid phase
361 separation together with a subset of COPII components[21,52]. Sec bodies are proposed to act
362 as temporal reservoirs for COPII components when secretion is blocked in response to
363 stress, that is immediately resolved upon stress removal[52]. Although yeast meiosis is a
364 process triggered by starvation, our results have shown that ERES are reduced in number
365 but do not undergo the feature of membrane-less structures; ERES remain active during
366 meiosis.

367 Gametogenesis in budding yeast regulates spore number by controlling catabolic
368 and anabolic pathways with available nutrients in response to starvation. In this situation,
369 the cell shuts off an energy-consuming secretory pathway at the ERES early in meiosis,
370 then lifting constraints by Gip1 in the later stage. However, the cell may take the strategy of
371 on membrane traffic only to produce a minimum number of spores, and Gip1 acts in this
372 process. This means that the cell maximizes usage of limited resources, initiating
373 membrane formation only at selected SPBs, and producing the determined number of
374 spores.

375 King et al. found that the mechanism of cell rejuvenation following sporulation is
376 achieved through the elimination of senescence factors such as non-chromosomal rDNA
377 circles with nuclear pore complexes from the gametes, and that PSMs are key for this
378 elimination[26]. In the present study, we found PP1-Gip1-triggered reorganization of
379 membrane traffic specifically in the cytoplasmic space engulfed by PSMs, and cells may use
380 this mechanism to eliminate senescence factors. The ERES has an important function not
381 only on the cytoplasmic side but also on the luminal side, which is to sort and filter the
382 transport cargo from ER-resident proteins[53]. Assuming that the bulky cargo and its receptor
383 are loaded into a COPII container to filter the ER-resident proteins by creating molecular
384 crowding[54], Sma2, its cargo receptor Erv14, and GPI-anchored proteins, including Spo19
385 and Cwp1[35,37], as a whole may play such a role. The work by Otto et al.[23] and our
386 observations indicate that a large fraction of the ER is left outside of nascent gametes upon
387 ER remodeling in meiosis. In this case, molecular crowding by the aforementioned bulky
388 cargo may contribute to the filtration of senescence factors, a subset of ER-PM tethers, left
389 behind from the lumen and membrane regions of the ER that are inherited by the gametes.

390 Our study provides a framework for the reorganization of membrane traffic during
391 meiosis to form PSMs. This elaborate maneuver not only generates *de novo* membrane
392 structures but also partitions the ERES, the Golgi, and ultimately the entire membrane traffic
393 itself into new cytosolic compartments created by the PSM. Importantly, a comparison of
394 lipid supply to the PSM with autophagosome and acrosome membrane formation points to

395 the fact that these membrane structures are generally cup-shaped bilayer structures with a
396 lumen, derived from vesicles from the Golgi, and their growth is directly mediated by lipid
397 transporters including Vps13 and Atg2[55,56]. During the formation of the autophagosomes,
398 the proximity of the autophagosomal isolation membrane to the ERES has been observed,
399 and direct fusion of COPII vesicles has also been proposed as a source of membrane
400 lipids[57,58]. Thus, the cell can utilize various strategies to assemble nascent membranes from
401 scratch. Identifying these individual mechanisms and uncovering their shared features will
402 provide key insights into both areas.

403 **Materials and methods**

404 **Yeast strains and plasmids**

405 Standard genetic techniques were used unless otherwise noted. All strains used in
406 this study are derivatives of SK1. Strains and plasmids are listed in Table S1 and S2,
407 respectively. The following alleles and plasmids were constructed in previous studies:
408 *NDT80::hphNT1::*P_{4xlexA}*-9xMyc-NDT80* and *AUR1::*P_{ACT1}*-LexA-ER-haVP16::AUR1-C*[7],
409 *mTagBFP2-Spo20*$^{51-917}$, and *glc7-136*[28].

410 Deletion and tagging of genes at their endogenous loci were performed by
411 standard PCR-based methods[58–61]. The pNC160-GFP-*GLC7* was a gift from K. Tatchell[62].

412 To construct *pRS306-mCherry-Spo20*$^{51-91}$ as a marker for PSM, sequences for
413 mCherry and a fragment of Spo20 were cloned into a *URA3* integrating vector harboring the
414 *TEF1* promoter and *DIT1* terminator. For the visualization of nucleus, *Htb2-mCherry*[10] was
415 cloned into *URA3* integrating vector. To generate *pRS303-mNG-Scs2TM*, sequences for
416 mNeonGreen and a transmembrane domain of Scs2 were cloned into the *HIS3* integrating
417 vector harboring the *TEF1* promoter and *DIT1* terminator. The full-length gene including
418 upstream and downstream flanking regions encoding *GIP1* was cloned into the *HIS3 CEN*
419 vector. To construct *HIS3* integration plasmids harboring either full-length *GIP1* or *GIP1*Δ*sep*,
420 corresponding sequences from *CEN TRP1* plasmids[27] were digested and cloned into
421 pRS303. All *HIS3* integration plasmids were integrated into the genome by BssHII digestion.
422 Similarly, *URA3* integration constructs were integrated by cutting with EcoRV. Coding
423 sequences for Sed4 or Sed4 without the luminal domain were cloned into the *HIS3*
424 integration vector together with upstream and downstream flanking regions, and
425 transformed into *sed4*Δ*::kanMX6* strains.

426

427 **Growth conditions**

428 Unless otherwise noted, standard media were used[63]. Induction of sporulation was
429 performed essentially as described[6]. Synchronous sporulation induction by the
430 estradiol-inducible *NDT80* block/release system was carried out as described previously[7,64].

431

432 **Fluorescence microscopy and image analyses**

433 Static images were acquired with a Leica Thunder Imager Live Cell equipped with
434 a Leica HC APO 100x oil immersion lens (NA 1.4), sCMOS camera DFC9000 GTC, as well
435 as by using a Keyence BZ-X710. Time-lapse imaging was performed with a super-resolution
436 confocal live imaging microscopy (SCLIM2), which we developed based on our basic
437 imaging system SCLIM[29,30]. This system consists of a Nikon ECLIPSE Ti2-E inverted
438 microscope equipped with a NIKON APO TIRF 100x NA 1.49 oil immersion objective lens, a

439 high-speed spinning-disk confocal scanner (CSU-X1, Yokogawa Electric), a custom-made
440 spectroscopic unit, an image intensifier (Hamamatsu Photonics) with a custom-made
441 cooling system, and three sCMOS cameras (Zyla 5.5, Andor) for green, red, and infrared
442 observation. Image acquisition was executed by NIS-Elements (Nikon). For 3D (*xyz*) and 4D
443 (*xyz* plus time) observations, cells induced for sporulation were immobilized on a
444 glass-based dish (Iwaki) by sandwiching with a 1% agarose pad containing 1% KOAc and
445 imaged. Stacks of ~ 50 image planes were collected with a spacing of 0.2 μm to cover the
446 entire cell. Z-stack images were subjected to deconvolution (iterative restoration) with
447 Volocity software (Perkin Elmer) using the theoretical point-spread function for spinning-disk
448 confocal microscopy, then combined using maximum intensity z-projection.
449
450 **Image quantification**
451 Intensity profile images for Sec13-GFP were obtained using the Metamorph built-in
452 module (Molecular Devices). For the quantification analysis of ERES numbers, Sec13-GFP
453 images were segmented into background and objects using the ilastik pixel classification
454 workflow[65]. Cell masks were also generated from bright field images using CellPose[66].
455 Distribution of the numbers for segmented ERES pixels within the area of the cell was
456 analyzed by Fiji and custom script in R. PSM perimeter was analyzed by Fiji. For
457 time-course analysis of ERES intensities, the PSM of interest was tracked manually and
458 fluorescent intensity (F_{PSM}) for the green channel was averaged within the region for PSM
459 and normalized to averaged fluorescent intensity of the whole cell (F_{cell}) over time.
460
461 **FRAP analysis**
462 FRAP analysis was performed using confocal laser scanning microscopy (LSM880,
463 Carl Zeiss) with a 63x Apochromat objective lens (NA 1.4) and a 488-nm laser. The
464 bleaching routine started with 2 pre-bleach scans followed by a bleaching scan, and the
465 recovery of fluorescence was monitored every 1 s for 60 s at 0.2% laser intensity. The
466 fluorescence recovery data were normalized using data acquired from the non-bleached
467 regions. Data were fitted to a double exponential curve to calculate half-time to recovery
468 after full scale normalization using easyFRAP software[67].
469
470 **Acknowledgement**
471 We are grateful to Aaron Neiman for fruitful discussion on this manuscript and all the
472 encouragement through the project. We thank all the members of Molecular Biology
473 Laboratory at Tsukuba University and Live Cell Super-Resolution Imaging Research Teams
474 at RIKEN Center for Advanced Photonics for discussions. We also thank to Kalai Madhi

Muniandy and Miho Waga for technical assistance. This work was supported by Grants-in-Aid for Scientific Research from the Ministry of Education, Culture, Sports, Science, and Technology (MEXT) of Japan (grant numbers 21K06145 to Y.S., 20K05782 and 23K05006 to H.T., 18H05275 to A.N., 22K06074 to K.I.).

Author contributions

Conceptualization: Y.S.

Formal analysis: Y.S. and T.S.

Investigation: Y.S. and T.S.

Resource: H.T.

Writing-Original Draft: Y.S.

Writing-Review & Editing: Y.S., H.T., K.K., A.N., and K.I.

Visualization: Y.S. and T.S.

Declaration of interests

The authors declare no competing financial interests.

491 **Figure legends**

492 **Figure 1**

493 Distribution of ERES numbers in meiotic progression. (A) Maximum intensity projections
494 (top) or single planes at the center (middle) or periphery (bottom) of cells expressing
495 mNG-Scs2TM and Htb2-mCherry at each time point in meiosis. Detachment of cortical ER
496 (closed arrowhead), expansion of cytoplasmic ER (open arrowhead), and regeneration of
497 cortical ER within the spores (arrow) are shown. (B) Single planes at the periphery (upper
498 left) or center (upper right) of vegetative and sporulating cells expressing Sec13-GFP. Signal
499 intensity profiles for Sec13-GFP in vegetative and sporulating cells (bottom). (C) Maximum
500 intensity projections of cells expressing Sec13-GFP with either Htb2-mCherry or
501 mCherry-Spo20$^{51-91}$ at each time point after induction of meiosis. (D) Quantification of the
502 experiments in upper images of panel C. Median is shown as dots. (E) Regeneration of
503 ERES in presumptive spore. Time-lapse images of single presumptive spores from cells
504 expressing Sec13-GFP and mCherry-Spo20$^{51-91}$ in meiosis. Kymograph from Movie S1 is
505 shown.

506

507 **Movie S1**

508 Dynamics of Sec13-GFP and mCherry-Spo20$^{51-91}$ in wild-type cell, related to Figure 1E.

509

510 **Figure S1**

511 (A) Montage of cells expressing Sec13-GFP and Htb2-mCherry in meiotic progression.
512 Quantification of Sec13-GFP signal intensity over time is also shown. Median is shown as a
513 bold line. (B) Quantification of signal intensity of Sec13-GFP per cell over time. (C)
514 Maximum intensity projections of the cells expressing Sec16-2xyEGFP, mCherry-Spo20$^{51-91}$
515 in meiosis. (D) Maximum intensity projections of the cells expressing Sec16-2xyEGFP,
516 Sec13-2xmCherry, and tagBFP-Spo20$^{51-91}$ in meiosis. (E) FRAP analysis of Sec13-GFP at
517 ERES in vegetatively growing or sporulating cells. Bleached area (circle) is shown in single
518 plane images of the upper left. Data represents in the upper right, mean ± SEM, n≥10.
519 Montage of Sec13-GFP recoveries is shown in the bottom panels. (F) Quantification of
520 half-time recoveries of the cells in vegetative growth or in each stage of meiotic progression.

521

522 **Figure 2**

523 Regeneration of the Golgi in presumptive spores. (A-C) Upper panels depict the markers of
524 distinct cisternae of the Golgi in budding yeast. (A) *cis*-Golgi localized enzyme Mnn9-sfGFP
525 or (B) *trans*-Golgi/TGN localized transmembrane protein Sys1-Envy or (C) *trans*-Golgi/TGN
526 localized peripheral marker Sec7-Envy. Middle panels showing maximum intensity

527 projections of the cells expressing Golgi makers with PSM marker mCherry-Spo20$^{51-91}$ at
528 each stage of PSM progression. Lower graphs depict quantification of middle panels. The
529 proportion of cells with or without Golgi signals or with Golgi localized signals in the spore
530 cytoplasm was analyzed.
531
532 **Figure 3**
533 ER-shaping determinants are important for the distribution of ERES numbers in meiosis.
534 (A-B) Maximum intensity projections of anaphase II cells expressing (A) mNG-Scs2TM and
535 Htb2-mCherry or (B) mNG-Scs2TM and mCherry-Spo20$^{51-91}$. (C) Maximum intensity
536 projections of cells expressing Sec13-GFP with mCherry-Spo20$^{51-91}$ at each time point after
537 induction of meiosis. Lower graph shows quantification of the experiments in the upper
538 panels. Median is shown as dots.
539
540 **Figure 4**
541 Gip1, a sporulation-specific PP1 targeting subunit, is required for ERES capture by PSMs.
542 (A) Maximum intensity projections of cells with the horseshoe-stage of PSMs expressing
543 Sec13-GFP with mCherry-Spo20$^{51-91}$ in mutants defective for PSM growth, *gip1*Δ, *gip1*Δ
544 with *CEN-GIP1*, *spo71*Δ, *spo73*Δ, or *vps13*Δ. (B) Quantification of the experiments in panel
545 A. (C) Maximum intensity projections of mutant cells, *gip1*Δ and *vps13*Δ, expressing
546 Sec13-GFP with mCherry-Spo20$^{51-91}$ at each time point after induction of meiosis. Lower
547 graphs show quantification of the experiments in upper panels. Median is shown as dots.
548 (D) Representative maximum intensity projection images of wild-type and *gip1*Δ cells
549 expressing mCherry-Spo20$^{51-91}$ at various stages of PSM growth. Numbers indicate
550 average cell perimeter. Quantification of the distributions of PSM length per cell at each time
551 point is shown in the right. (E) Quantification of the distribution of PSM length and ERES
552 acquisition per cell at 7-8 hours after meiosis induction in wild-type and *gip1*Δ.
553
554 **Figure 5**
555 Gip1-dependent regeneration of ERES within presumptive spores. (A) Representative
556 time-lapse image of single presumptive spores from *gip1*Δ cells expressing Sec13-GFP and
557 mCherry-Spo20$^{51-91}$ in meiosis. Kymograph from Movie S2 is shown. (B) Quantification of
558 signal intensities of ERES, Sec13-GFP in the cytoplasm of single PSMs of wild-type and
559 *gip1*Δ cells over time. (C) Maximum intensity projection images of anaphase II cells
560 depicting the ER marked with mNG-Scs2TM and PSMs, mCherry-Spo20$^{51-91}$ in wild-type
561 and *gip1*Δ. (D) Maximum intensity projections of *gip1*Δ cells expressing Mnn9-sfGFP,
562 Sys1-Envy, or Sec7-Envy, with PSM marker mCherry-Spo20$^{51-91}$ at each stage of PSM

563 progression.
564
565 **Movie S2**
566 Dynamics of Sec13-GFP and mCherry-Spo20$^{51-91}$ in *gip1*Δ cell, related to Figure 5A.
567
568 **Figure 6**
569 Gip1-dependent foci formation of Sec16 at the onset of PSM formation. (A-B) Maximum
570 intensity projections of cells with various stages of PSMs expressing GFP-Glc7 with
571 mCherry-Spo20$^{51-91}$ in wild-type (A) and *gip1*Δ (B). (C) Representative maximum intensity
572 projection image of Sec13-GFP and mCherry-Spo20$^{51-91}$ in *glc7-136* cells, in which the
573 association between Glc7, the catalytic subunit of PP1, and Gip1, a development-specific
574 targeting subunit of PP1, is defective. (D-E) Maximum intensity projections of cells at
575 indicated stages during meiotic progression. Wild-type and *gip1*Δ cells expressing
576 Sec16-2xyEGFP with (D) Htb2-mCherry or (E) mCherry-Spo20$^{51-91}$. (F) Quantification of the
577 experiments shown in panels D and E.
578
579 **Figure S2**
580 Gip1 contributes to ERES regeneration localizing only in the vicinity of PSMs. Quantification
581 of ERES regeneration in presumptive spores in *gip1*Δ cells expressing full-length Gip1 or
582 Gip1Δsep lacking the septin localization domain.
583
584 **Figure 7**
585 Deletion of *SED4* phenocopied most of the defects observed in *gip1*Δ cells. (A)
586 Representative bright field images of wild-type and *sed4*Δ cells that were induced to
587 sporulate. Graph shows the quantification of the distribution of asci in left panels. (B)
588 Representative images of GFP-Sec12 or GFP-Sed4 with mCherry-Spo20$^{51-91}$ at each stage
589 of meiosis in wild-type cells. (C) Maximum intensity projection images of cells with
590 Sec13-GFP and mCherry-Spo20$^{51-91}$ in *sed4*Δ harboring empty vector, full-length *SED4*, or
591 *SED4* lacking the luminal domain (*SED4*Δ*lum*). (D) Quantification of the PSM perimeters in
592 wild-type, *gip1*Δ, and *sed4*Δ. (E) Representative time-lapse image of single presumptive
593 spores from *sed4*Δ cells expressing Sec13-GFP and mCherry-Spo20$^{51-91}$ in meiosis.
594 Kymograph from Movie S3 is shown. (F) Quantification of signal intensities of ERES,
595 Sec13-GFP in the cytoplasm of single PSMs of wild-type and *gip1*Δ cells over time.
596
597 **Movie S3**
598 Dynamics of Sec13-GFP and mCherry-Spo20$^{51-91}$ in *sed4*Δ cell, related to Figure 7E.

599

600 **Figure 8**

601 Model for the early step of PSM formation. Coalescence and fusion of post-Golgi vesicles
602 initiate nascent PSMs at SPBs. ERES formation is transiently inactivated during meiosis
603 (ERES in grey), while ERES regeneration is locally activated in the region surrounded by the
604 PSM in early anaphase II (ERES in orange). Gip1-Glc7 mediates ERES regeneration, Golgi
605 re-assembly, and presumably supplies membrane lipids toward PSMs via membrane traffic.
606 Gip1-Glc7 is also essential for septin high-order structural formation in the spore cytoplasm.
607 In this step, the Vps13-complex functions as the direct lipid conduit from the ER to PSMs.

608

609 **References**

610 1. Neiman, A.M. (2011). Sporulation in the Budding Yeast Saccharomyces cerevisiae.
611 Genetics *189*, 737–765. 10.1534/genetics.111.127126.

612 2. Sing, T.L., Brar, G.A., and Ünal, E. (2022). Gametogenesis: Exploring an Endogenous
613 Rejuvenation Program to Understand Cellular Aging and Quality Control. Annu. Rev.
614 Genet. *56*, 89–112. 10.1146/annurev-genet-080320-025104.

615 3. Renicke, C., Allmann, A.-K., Lutz, A.P., Heimerl, T., and Taxis, C. (2017). The Mitotic
616 Exit Network Regulates Spindle Pole Body Selection During Sporulation of
617 Saccharomyces cerevisiae. Genetics *206*, 919–937. 10.1534/genetics.116.194522.

618 4. Taxis, C., Keller, P., Kavagiou, Z., Jensen, L.J., Colombelli, J., Bork, P., Stelzer, E.H.K.,
619 and Knop, M. (2005). Spore number control and breeding in Saccharomyces
620 cerevisiae: a key role for a self-organizing system. J. Cell Biol. *171*, 627–640.
621 10.1083/jcb.200507168.

622 5. Neiman, A.M. (2005). Ascospore formation in the yeast Saccharomyces cerevisiae.
623 Microbiol. Mol. Biol. Rev. *69*, 565–584. 10.1128/MMBR.69.4.565-584.2005.

624 6. Neiman, A.M. (1998). Prospore membrane formation defines a developmentally
625 regulated branch of the secretory pathway in yeast. J. Cell Biol. *140*, 29–37.
626 10.1083/jcb.140.1.29.

627 7. Nakamura, T.S., Suda, Y., Muneshige, K., Fujieda, Y., Okumura, Y., Inoue, I., Tanaka, T.,
628 Takahashi, T., Nakanishi, H., Gao, X.-D., et al. (2021). Suppression of Vps13 adaptor
629 protein mutants reveals a central role for PI4P in regulating prospore membrane
630 extension. PLoS Genet. *17*, e1009727. 10.1371/journal.pgen.1009727.

631 8. Park, J.-S., Okumura, Y., Tachikawa, H., and Neiman, A.M. (2013). SPO71 encodes a
632 developmental stage-specific partner for Vps13 in Saccharomyces cerevisiae. Eukaryot.
633 Cell *12*, 1530–1537. 10.1128/EC.00239-13.

634 9. Parodi, E.M., Roesner, J.M., and Huang, L.S. (2015). SPO73 and SPO71 Function
635 Cooperatively in Prospore Membrane Elongation During Sporulation in Saccharomyces
636 cerevisiae. PLoS One *10*, e0143571. 10.1371/journal.pone.0143571.

637 10. Okumura, Y., Nakamura, T.S., Tanaka, T., Inoue, I., Suda, Y., Takahashi, T., Nakanishi,
638 H., Nakamura, S., Gao, X.-D., and Tachikawa, H. (2016). The Dysferlin Domain-Only

639 Protein, Spo73, Is Required for Prospore Membrane Extension in Saccharomyces
640 cerevisiae. mSphere *1*. 10.1128/mSphere.00038-15.

641 11. Park, J.-S., Thorsness, M.K., Policastro, R., McGoldrick, L.L., Hollingsworth, N.M.,
642 Thorsness, P.E., and Neiman, A.M. (2016). Yeast Vps13 promotes mitochondrial
643 function and is localized at membrane contact sites. Mol. Biol. Cell *27*, 2435–2449.
644 10.1091/mbc.E16-02-0112.

645 12. Adlakha, J., Hong, Z., Li, P.Q., and Reinisch, K.M. (2022). Structural and biochemical
646 insights into lipid transport by VPS13 proteins. J. Cell Biol. *221*.
647 10.1101/2022.03.11.484024.

648 13. Hammond, A.T., and Glick, B.S. (2000). Dynamics of transitional endoplasmic reticulum
649 sites in vertebrate cells. Mol. Biol. Cell *11*, 3013–3030. 10.1091/mbc.11.9.3013.

650 14. Lord, C., Ferro-Novick, S., and Miller, E.A. (2013). The highly conserved COPII coat
651 complex sorts cargo from the endoplasmic reticulum and targets it to the golgi. Cold
652 Spring Harb. Perspect. Biol. *5*. 10.1101/cshperspect.a013367.

653 15. Okamoto, M., Kurokawa, K., Matsuura-Tokita, K., Saito, C., Hirata, R., and Nakano, A.
654 (2012). High-curvature domains of the ER are important for the organization of ER exit
655 sites in Saccharomyces cerevisiae. J. Cell Sci. *125*, 3412–3420. 10.1242/jcs.100065.

656 16. Bharucha, N., Liu, Y., Papanikou, E., McMahon, C., Esaki, M., Jeffrey, P.D., Hughson,
657 F.M., and Glick, B.S. (2013). Sec16 influences transitional ER sites by regulating rather
658 than organizing COPII. Mol. Biol. Cell *24*, 3406–3419. 10.1091/mbc.E13-04-0185.

659 17. Hughes, H., Budnik, A., Schmidt, K., Palmer, K.J., Mantell, J., Noakes, C., Johnson, A.,
660 Carter, D.A., Verkade, P., Watson, P., et al. (2009). Organisation of human ER-exit
661 sites: requirements for the localisation of Sec16 to transitional ER. J. Cell Sci. *122*,
662 2924–2934. 10.1242/jcs.044032.

663 18. Sprangers, J., and Rabouille, C. (2015). SEC16 in COPII coat dynamics at ER exit sites.
664 Biochem. Soc. Trans. *43*, 97–103. 10.1042/BST20140283.

665 19. Maeda, M., Komatsu, Y., and Saito, K. (2020). Mitotic ER Exit Site Disassembly and
666 Reassembly Are Regulated by the Phosphorylation Status of TANGO1. Dev. Cell *55*,
667 237-250.e5. 10.1016/j.devcel.2020.07.017.

668 20. Maeda, M., Komatsu, Y., and Saito, K. (2020). Mitotic ER exit site dynamics: insights

669 into blockade of secretion from the ER during mitosis. Mol Cell Oncol *7*, 1832420.
670 10.1080/23723556.2020.1832420.

671 21. Zacharogianni, M., Aguilera-Gomez, A., Veenendaal, T., Smout, J., and Rabouille, C.
672 (2014). A stress assembly that confers cell viability by preserving ERES components
673 during amino-acid starvation. Elife *3*. 10.7554/eLife.04132.

674 22. Suda, Y., Nakanishi, H., Mathieson, E.M., and Neiman, A.M. (2007). Alternative modes
675 of organellar segregation during sporulation in Saccharomyces cerevisiae. Eukaryot.
676 Cell *6*, 2009–2017. 10.1128/EC.00238-07.

677 23. Otto, G.M., Cheunkarndee, T., Leslie, J.M., and Brar, G.A. (2021). Programmed cortical
678 ER collapse drives selective ER degradation and inheritance in yeast meiosis. J. Cell
679 Biol. *220*. 10.1083/jcb.202108105.

680 24. Sawyer, E.M., Joshi, P.R., Jorgensen, V., Yunus, J., Berchowitz, L.E., and Ünal, E.
681 (2019). Developmental Regulation of an Organelle Tether Coordinates Mitochondrial
682 Remodeling in Meiosis. J. Cell Biol. *218*, 559–579. 10.1083/jcb.201807097.

683 25. Goodman, J.S., King, G.A., and Ünal, E. (2020). Cellular quality control during
684 gametogenesis. Exp. Cell Res. *396*, 112247. 10.1016/j.yexcr.2020.112247.

685 26. King, G.A., Goodman, J.S., Schick, J.G., Chetlapalli, K., Jorgens, D.M., McDonald, K.L.,
686 and Ünal, E. (2019). Meiotic cellular rejuvenation is coupled to nuclear remodeling in
687 budding yeast. Elife *8*. 10.7554/eLife.47156.

688 27. Nakamura, T.S., Numajiri, Y., Okumura, Y., Hidaka, J., Tanaka, T., Inoue, I., Suda, Y.,
689 Takahashi, T., Nakanishi, H., Gao, X.-D., et al. (2017). Dynamic localization of a yeast
690 development-specific PP1 complex during prospore membrane formation is dependent
691 on multiple localization signals and complex formation. Mol. Biol. Cell *28*, 3881–3895.
692 10.1091/mbc.E17-08-0521.

693 28. Tachikawa, H., Bloecher, A., Tatchell, K., and Neiman, A.M. (2001). A Gip1p-Glc7p
694 phosphatase complex regulates septin organization and spore wall formation. J. Cell
695 Biol. *155*, 797–808. 10.1083/jcb.200107008.

696 29. Kurokawa, K., Ishii, M., Suda, Y., Ichihara, A., and Nakano, A. (2013). Live cell
697 visualization of Golgi membrane dynamics by super-resolution confocal live imaging
698 microscopy. Methods Cell Biol. *118*, 235–242. 10.1016/B978-0-12-417164-0.00014-8.

699 30. Tojima, T., Miyashiro, D., Kosugi, Y., and Nakano, A. (2023). Super-Resolution Live
700 Imaging of Cargo Traffic Through the Golgi Apparatus in Mammalian Cells. Methods
701 Mol. Biol. *2557*, 127–140. 10.1007/978-1-0716-2639-9_10.

702 31. Glick, B.S. (2002). Can the Golgi form de novo? Nat. Rev. Mol. Cell Biol. *3*, 615–619.
703 10.1038/nrm877.

704 32. Kurokawa, K., Osakada, H., Kojidani, T., Waga, M., Suda, Y., Asakawa, H., Haraguchi,
705 T., and Nakano, A. (2019). Visualization of secretory cargo transport within the Golgi
706 apparatus. J. Cell Biol. *218*, 1602–1618. 10.1083/jcb.201807194.

707 33. Tojima, T., Suda, Y., Ishii, M., Kurokawa, K., and Nakano, A. (2019). Spatiotemporal
708 dissection of the trans-Golgi network in budding yeast. J. Cell Sci. *132*.
709 10.1242/jcs.231159.

710 34. Chen, S., Novick, P., and Ferro-Novick, S. (2013). ER structure and function. Curr. Opin.
711 Cell Biol. *25*, 428–433. 10.1016/j.ceb.2013.02.006.

712 35. Nakanishi, H., Suda, Y., and Neiman, A.M. (2007). Erv14 family cargo receptors are
713 necessary for ER exit during sporulation in Saccharomyces cerevisiae. J. Cell Sci. *120*,
714 908–916. 10.1242/jcs.03405.

715 36. Parodi, E.M., Baker, C.S., Tetzlaff, C., Villahermosa, S., and Huang, L.S. (2012).
716 SPO71 mediates prospore membrane size and maturation in Saccharomyces
717 cerevisiae. Eukaryot. Cell *11*, 1191–1200. 10.1128/EC.00076-12.

718 37. Maier, P., Rathfelder, N., Maeder, C.I., Colombelli, J., Stelzer, E.H.K., and Knop, M.
719 (2008). The SpoMBe pathway drives membrane bending necessary for cytokinesis and
720 spore formation in yeast meiosis. EMBO J. *27*, 2363–2374. 10.1038/emboj.2008.168.

721 38. Baker, S.H., Frederick, D.L., Bloecher, A., and Tatchell, K. (1997). Alanine-scanning
722 mutagenesis of protein phosphatase type 1 in the yeast Saccharomyces cerevisiae.
723 Genetics *145*, 615–626. 10.1093/genetics/145.3.615.

724 39. Gimeno, R.E., Espenshade, P., and Kaiser, C.A. (1995). SED4 encodes a yeast
725 endoplasmic reticulum protein that binds Sec16p and participates in vesicle formation.
726 J. Cell Biol. *131*, 325–338. 10.1083/jcb.131.2.325.

727 40. Saito-Nakano, Y., and Nakano, A. (2000). Sed4p functions as a positive regulator of
728 Sar1p probably through inhibition of the GTPase activation by Sec23p. Genes Cells *5*,

729 1039–1048. 10.1046/j.1365-2443.2000.00391.x.

730 41. Kodera, C., Yorimitsu, T., Nakano, A., and Sato, K. (2011). Sed4p stimulates Sar1p
731 GTP hydrolysis and promotes limited coat disassembly. Traffic *12*, 591–599.
732 10.1111/j.1600-0854.2011.01173.x.

733 42. Dubreuil, B., Sass, E., Nadav, Y., Heidenreich, M., Georgeson, J.M., Weill, U., Duan, Y.,
734 Meurer, M., Schuldiner, M., Knop, M., et al. (2019). YeastRGB: comparing the
735 abundance and localization of yeast proteins across cells and libraries. Nucleic Acids
736 Res. *47*, D1245–D1249. 10.1093/nar/gky941.

737 43. Kurokawa, K., Okamoto, M., and Nakano, A. (2014). Contact of cis-Golgi with ER exit
738 sites executes cargo capture and delivery from the ER. Nat. Commun. *5*, 3653.
739 10.1038/ncomms4653.

740 44. Yorimitsu, T., and Sato, K. (2020). Sec16 function in ER export and autophagy is
741 independent of its phosphorylation in Saccharomyces cerevisiae. MBoC *31*, 149–156.
742 10.1091/mbc.E19-08-0477.

743 45. Attner, M.A., Miller, M.P., Ee, L.-S., Elkin, S.K., and Amon, A. (2013). Polo kinase Cdc5
744 is a central regulator of meiosis I. Proc. Natl. Acad. Sci. U. S. A. *110*, 14278–14283.
745 10.1073/pnas.1311845110.

746 46. Argüello-Miranda, O., Zagoriy, I., Mengoli, V., Rojas, J., Jonak, K., Oz, T., Graf, P., and
747 Zachariae, W. (2017). Casein Kinase 1 Coordinates Cohesin Cleavage,
748 Gametogenesis, and Exit from M Phase in Meiosis II. Dev. Cell *40*, 37–52.
749 10.1016/j.devcel.2016.11.021.

750 47. Carlton, J.G., Jones, H., and Eggert, U.S. (2020). Membrane and organelle dynamics
751 during cell division. Nat. Rev. Mol. Cell Biol. *21*, 151–166. 10.1038/s41580-019-0208-1.

752 48. Yorimitsu, T., and Sato, K. (2023). Sec16 and Sed4 interdependently function as
753 interaction and localization partners at ER exit sites. J. Cell Sci. *136*.
754 10.1242/jcs.261094.

755 49. Ito, Y., Uemura, T., and Nakano, A. (2018). The Golgi entry core compartment functions
756 as a COPII-independent scaffold for ER-to-Golgi transport in plant cells. J. Cell Sci. *131*.
757 10.1242/jcs.203893.

758 50. Ito, Y., Uemura, T., Shoda, K., Fujimoto, M., Ueda, T., and Nakano, A. (2012). cis-Golgi

759 proteins accumulate near the ER exit sites and act as the scaffold for Golgi
760 regeneration after brefeldin A treatment in tobacco BY-2 cells. Mol. Biol. Cell *23*, 3203–
761 3214. 10.1091/mbc.E12-01-0034.

762 51. Ito, Y., and Boutté, Y. (2020). Differentiation of Trafficking Pathways at Golgi Entry Core
763 Compartments and Post-Golgi Subdomains. Front. Plant Sci. *11*, 609516.
764 10.3389/fpls.2020.609516.

765 52. van Leeuwen, W., Nguyen, D.T.M., Grond, R., Veenendaal, T., Rabouille, C., and Farías,
766 G.G. (2022). Stress-induced phase separation of ERES components into Sec bodies
767 precedes ER exit inhibition in mammalian cells. J. Cell Sci. 10.1242/jcs.260294.

768 53. Raote, I., Saxena, S., and Malhotra, V. (2022). Sorting and Export of Proteins at the
769 Endoplasmic Reticulum. Cold Spring Harb. Perspect. Biol.
770 10.1101/cshperspect.a041258.

771 54. Gomez-Navarro, N., Melero, A., Li, X.-H., Boulanger, J., Kukulski, W., and Miller, E.A.
772 (2020). Cargo crowding contributes to sorting stringency in COPII vesicles. J. Cell Biol.
773 *219*. 10.1083/jcb.201806038.

774 55. Melia, T.J., and Reinisch, K.M. (2022). A possible role for VPS13-family proteins in bulk
775 lipid transfer, membrane expansion and organelle biogenesis. J. Cell Sci. *135*.
776 10.1242/jcs.259357.

777 56. Da Costa, R., Bordessoules, M., Guilleman, M., Carmignac, V., Lhussiez, V., Courot, H.,
778 Bataille, A., Chlémaire, A., Bruno, C., Fauque, P., et al. (2020). Vps13b is required for
779 acrosome biogenesis through functions in Golgi dynamic and membrane trafficking.
780 Cell. Mol. Life Sci. *77*, 511–529. 10.1007/s00018-019-03192-4.

781 57. Graef, M., Friedman, J.R., Graham, C., Babu, M., and Nunnari, J. (2013). ER exit sites
782 are physical and functional core autophagosome biogenesis components. Mol. Biol.
783 Cell *24*, 2918–2931. 10.1091/mbc.E13-07-0381.

784 58. Suzuki, K., Akioka, M., Kondo-Kakuta, C., Yamamoto, H., and Ohsumi, Y. (2013). Fine
785 mapping of autophagy-related proteins during autophagosome formation in
786 Saccharomyces cerevisiae. J. Cell Sci. *126*, 2534–2544. 10.1242/jcs.122960.

787 59. Longtine, M.S., Mc KENZIE, A., Demarini, D.J., Shah, N.G., Wach, A., Brachat, A.,
788 Philippsen, P., and Pringle, J.R. (1998). Additional Modules for Versatile and
789 Economical PCR-based Gene Deletion and Modification in Saccharomyces cerevisiae.

790 Yeast *14*, 915–922.
791 10.1002/(SICI)1097-0061(199807)14:10<915::AID-YEA291>3.0.CO;2-Y.

792 60. Janke, C., Magiera, M.M., Rathfelder, N., Taxis, C., Reber, S., Maekawa, H.,
793 Moreno-Borchart, A., Doenges, G., Schwob, E., Schiebel, E., et al. (2004). A versatile
794 toolbox for PCR-based tagging of yeast genes: new fluorescent proteins, more markers
795 and promoter substitution cassettes. Yeast *21*, 947–962. 10.1002/yea.1142.

796 61. Khmelinskii, A., Meurer, M., Duishoev, N., Delhomme, N., and Knop, M. (2011).
797 Seamless gene tagging by endonuclease-driven homologous recombination. PLoS
798 One *6*, e23794. 10.1371/journal.pone.0023794.

799 62. Bloecher, A., and Tatchell, K. (2000). Dynamic localization of protein phosphatase type
800 1 in the mitotic cell cycle of Saccharomyces cerevisiae. J. Cell Biol. *149*, 125–140.
801 10.1083/jcb.149.1.125.

802 63. Burke, D., Dawson, D., and Stearns, T. (2000). Methods in yeast genetics: a Cold
803 Spring Harbor Laboratory course manual (2000 edition). Plainview, NY: Cold Spring
804 Harbor Laboratory Press. [Google Scholar].

805 64. Tio, C.W., Omerza, G., Sunder, S., and Winter, E. (2015). Autophosphorylation of the
806 Smk1 MAPK is spatially and temporally regulated by Ssp2 during meiotic development
807 in yeast. Mol. Biol. Cell *26*, 3546–3555. 10.1091/mbc.E15-05-0322.

808 65. Berg, S., Kutra, D., Kroeger, T., Straehle, C.N., Kausler, B.X., Haubold, C., Schiegg, M.,
809 Ales, J., Beier, T., Rudy, M., et al. (2019). ilastik: interactive machine learning for
810 (bio)image analysis. Nat. Methods *16*, 1226–1232. 10.1038/s41592-019-0582-9.

811 66. Stringer, C., Wang, T., Michaelos, M., and Pachitariu, M. (2021). Cellpose: a generalist
812 algorithm for cellular segmentation. Nat. Methods *18*, 100–106.
813 10.1038/s41592-020-01018-x.

814 67. Koulouras, G., Panagopoulos, A., Rapsomaniki, M.A., Giakoumakis, N.N., Taraviras, S.,
815 and Lygerou, Z. (2018). EasyFRAP-web: a web-based tool for the analysis of
816 fluorescence recovery after photobleaching data. Nucleic Acids Res. *46*, W467–W472.
817 10.1093/nar/gky508.

Figure 1

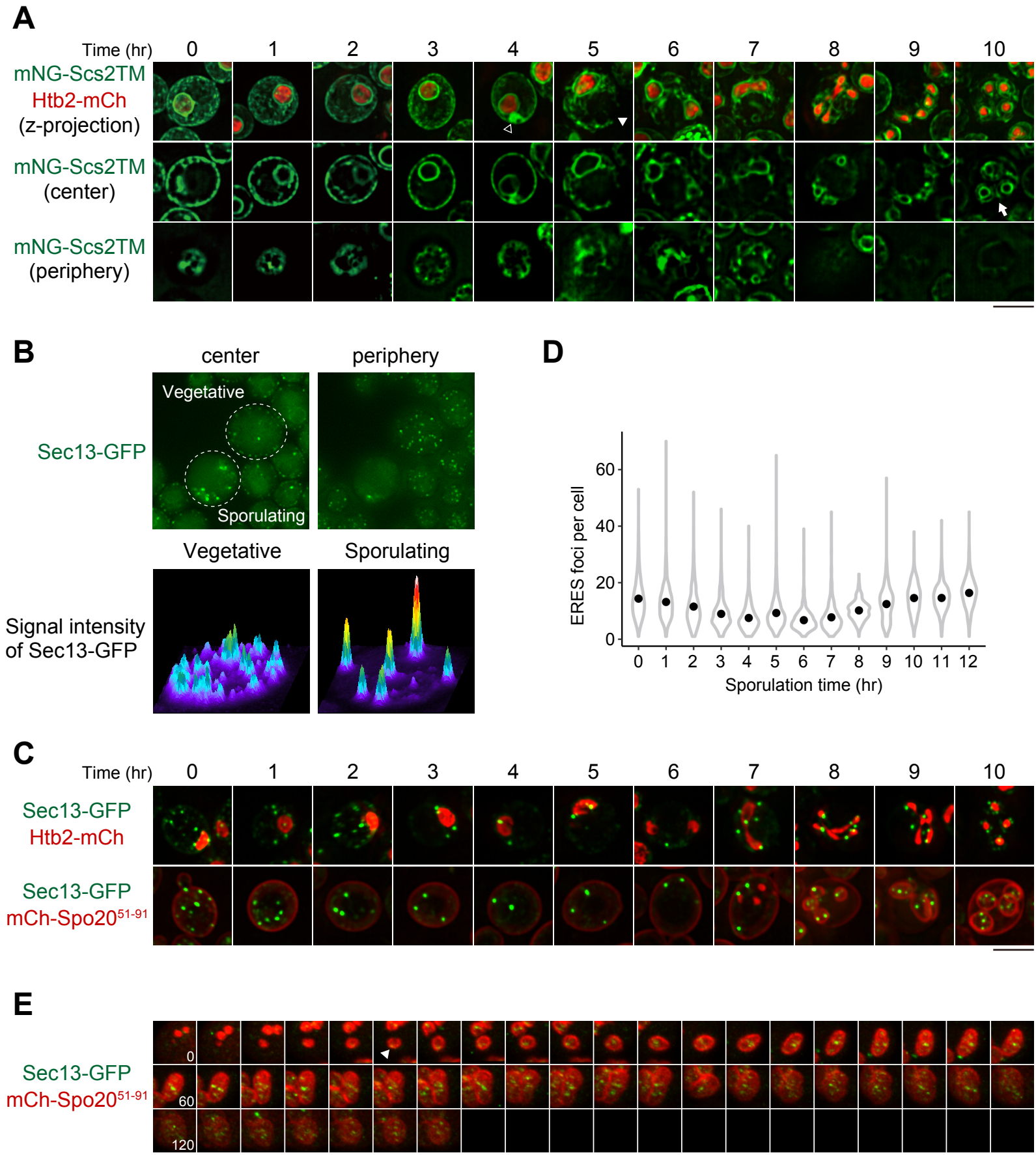
A
Time (hr)
0
1
2
3
4
5
6
7
8
9
10
mNG-Scs2TM
Htb2-mCh
(z-projection)
mNG-Scs2TM
(center)
mNG-Scs2TM
(periphery)
B
center
periphery
Vegetative
Sporulating
Sec13-GFP
Vegetative
Sporulating
Signal intensity
of Sec13-GFP
D
ERES foci per cell
0
20
40
60
0 1 2 3 4 5 6 7 8 9 10 11 12
Sporulation time (hr)
C
Time (hr)
0
1
2
3
4
5
6
7
8
9
10
Sec13-GFP
Htb2-mCh
Sec13-GFP
mCh-Spo20$^{51-91}$
E
Sec13-GFP
mCh-Spo20$^{51-91}$
0
60
120

Figure 2

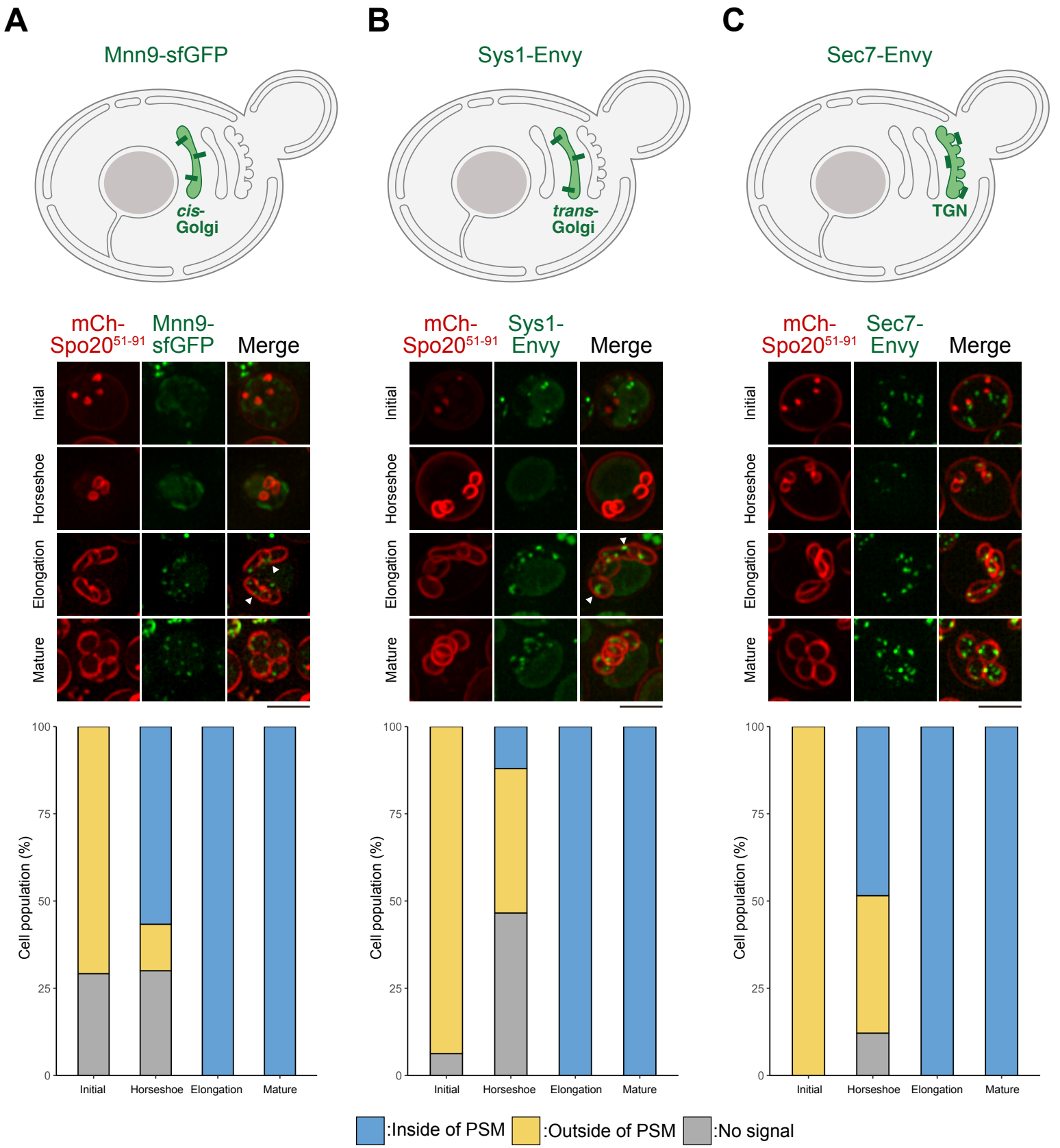
A
Mnn9-sfGFP
cis-
Golgi
B
Sys1-Envy
trans-
Golgi
C
Sec7-Envy
TGN
mCh-Spo20^51-91
Mnn9-sfGFP
Merge
mCh-Spo20^51-91
Sys1-Envy
Merge
mCh-Spo20^51-91
Sec7-Envy
Merge
Initial
Horseshoe
Elongation
Mature
Cell population (%)
100
75
50
25
0
Initial
Horseshoe
Elongation
Mature
:Inside of PSM
:Outside of PSM
:No signal

Figure 3

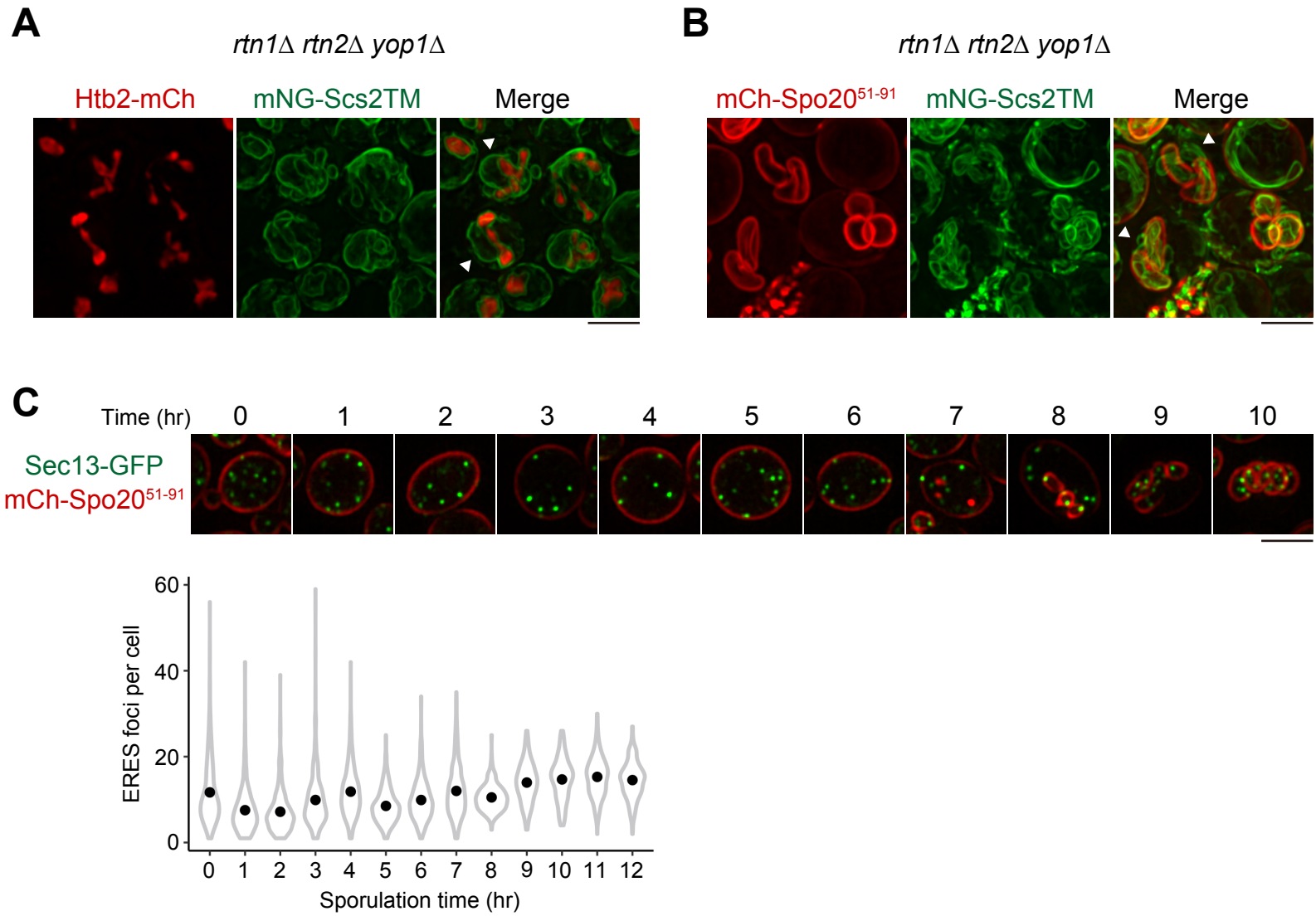
A
rtn1Δ rtn2Δ yop1Δ
Htb2-mCh
mNG-Scs2TM
Merge
B
rtn1Δ rtn2Δ yop1Δ
mCh-Spo20^51-91
mNG-Scs2TM
Merge
C
Time (hr)
0
1
2
3
4
5
6
7
8
9
10
Sec13-GFP
mCh-Spo20^51-91
ERES foci per cell
60
40
20
0
0 1 2 3 4 5 6 7 8 9 10 11 12
Sporulation time (hr)

Figure 4

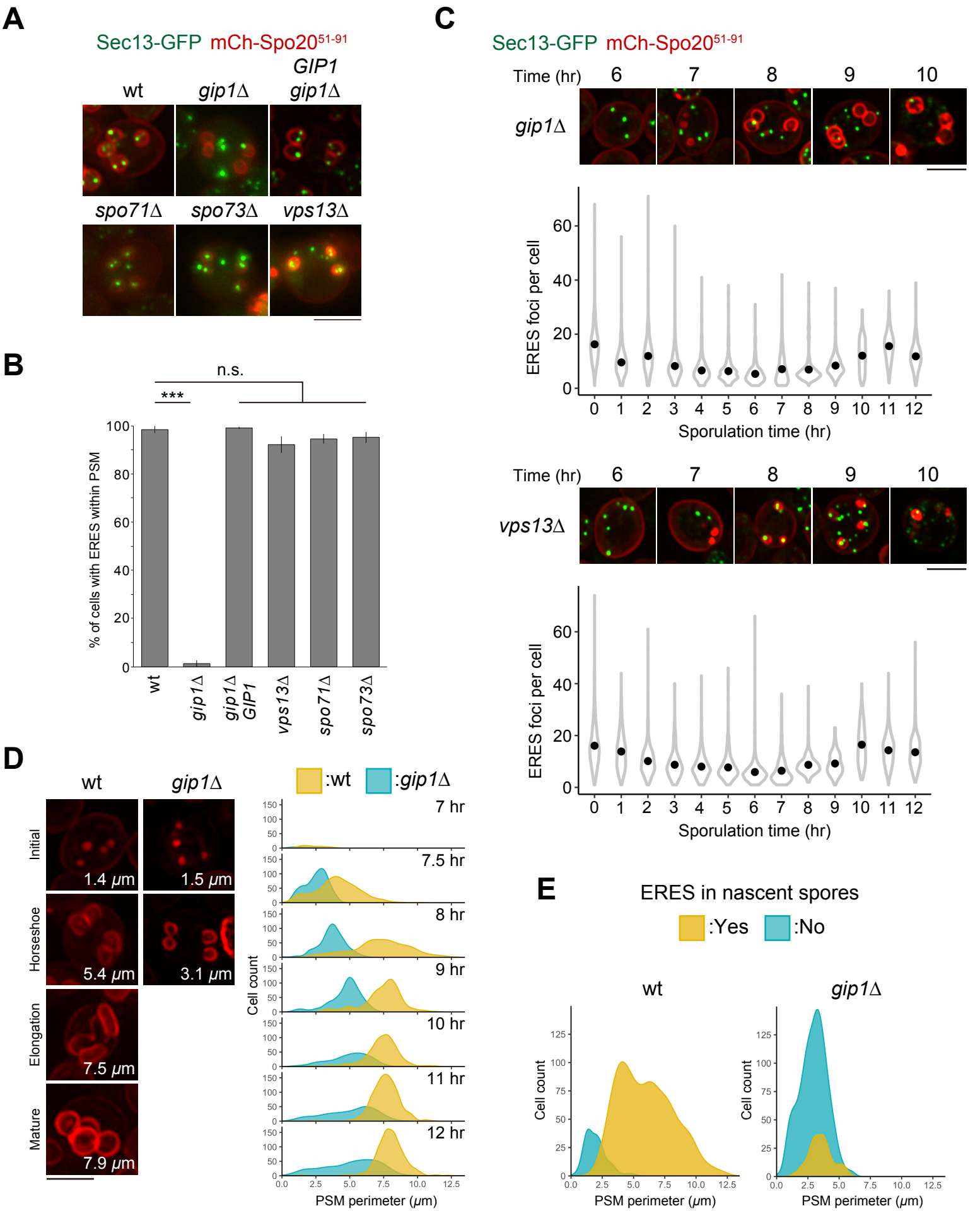
A
Sec13-GFP mCh-Spo20$^{51-91}$
wt
gip1Δ
GIP1 gip1Δ
spo71Δ
spo73Δ
vps13Δ
B
n.s.
***
% of cells with ERES within PSM
wt
gip1Δ
gip1Δ GIP1
vps13Δ
spo71Δ
spo73Δ
C
Sec13-GFP mCh-Spo20$^{51-91}$
Time (hr)
gip1Δ
vps13Δ
ERES foci per cell
Sporulation time (hr)
D
wt
gip1Δ
Initial
Horseshoe
Elongation
Mature
1.4 μm
1.5 μm
5.4 μm
3.1 μm
7.5 μm
7.9 μm
:wt
:gip1Δ
7 hr
7.5 hr
8 hr
9 hr
10 hr
11 hr
12 hr
Cell count
PSM perimeter (μm)
E
ERES in nascent spores
:Yes
:No
wt
gip1Δ
Cell count
PSM perimeter (μm)

Figure 5

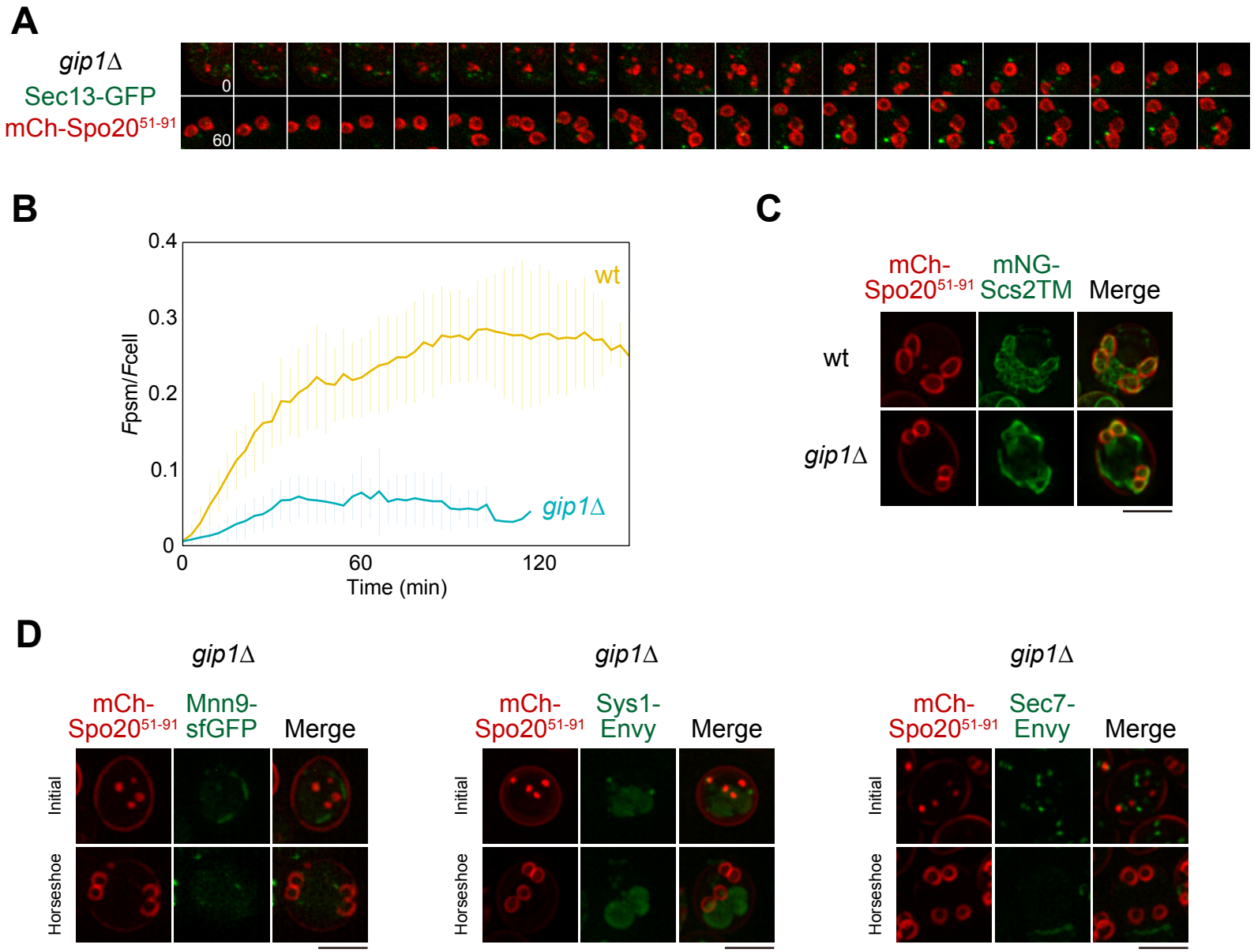
A
gip1Δ
Sec13-GFP
mCh-Spo20^51-91
0
60
B
0.4
0.3
0.2
0.1
0
Fpsm/Fcell
wt
gip1Δ
0
60
120
Time (min)
C
mCh-Spo20^51-91
mNG-Scs2TM
Merge
wt
gip1Δ
D
gip1Δ
mCh-Spo20^51-91
Mnn9-sfGFP
Merge
Initial
Horseshoe
gip1Δ
mCh-Spo20^51-91
Sys1-Envy
Merge
Initial
Horseshoe
gip1Δ
mCh-Spo20^51-91
Sec7-Envy
Merge
Initial
Horseshoe

Figure 6

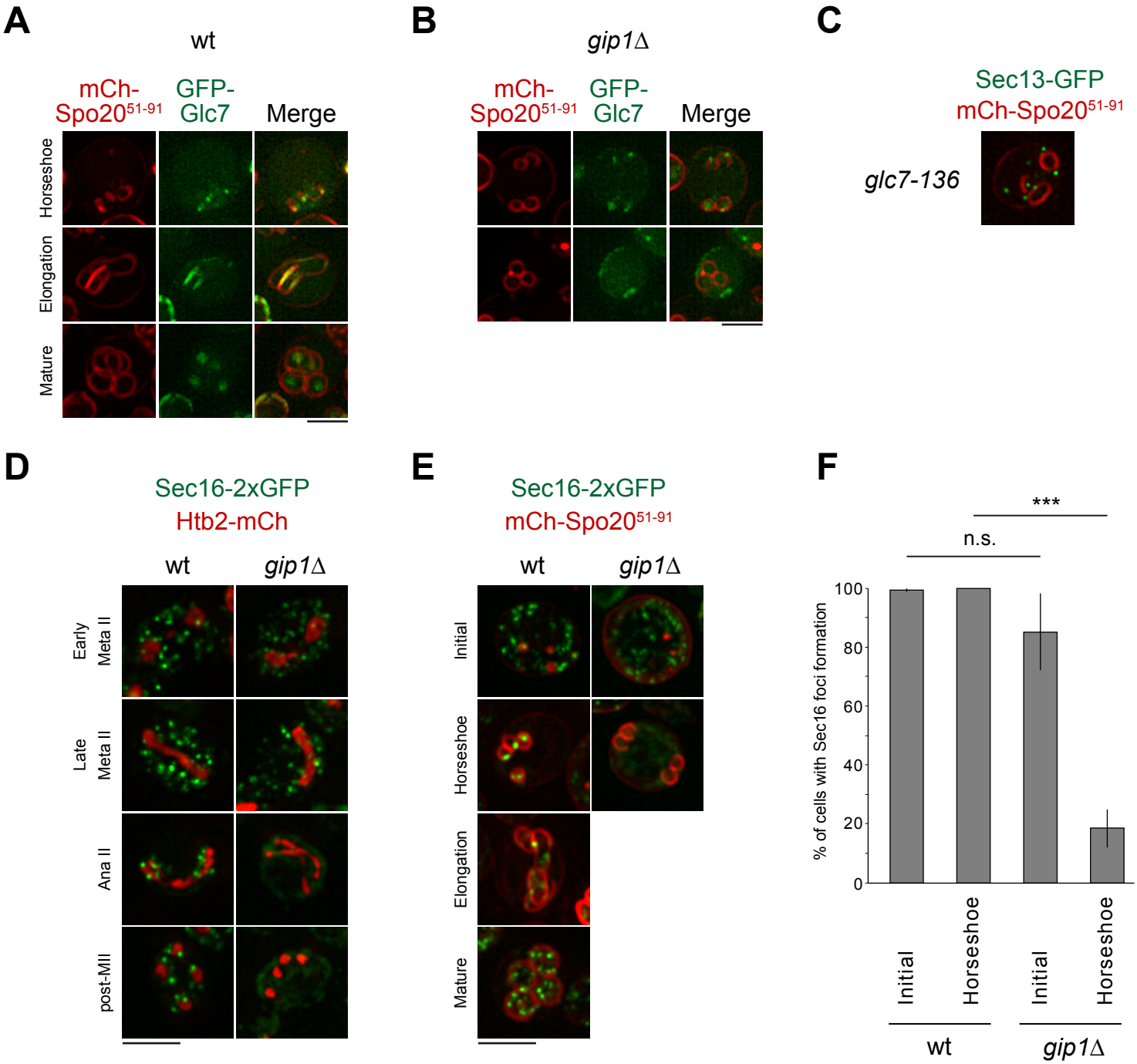
A
wt
mCh-Spo20$^{51-91}$
GFP-Glc7
Merge
Horseshoe
Elongation
Mature
B
gip1Δ
mCh-Spo20$^{51-91}$
GFP-Glc7
Merge
C
Sec13-GFP
mCh-Spo20$^{51-91}$
glc7-136
D
Sec16-2xGFP
Htb2-mCh
wt
gip1Δ
Early Meta II
Late Meta II
Ana II
post-MII
E
Sec16-2xGFP
mCh-Spo20$^{51-91}$
wt
gip1Δ
Initial
Horseshoe
Elongation
Mature
F
***
n.s.
% of cells with Sec16 foci formation
100
80
60
40
20
0
Initial
Horseshoe
Initial
Horseshoe
wt
gip1Δ

Figure 7

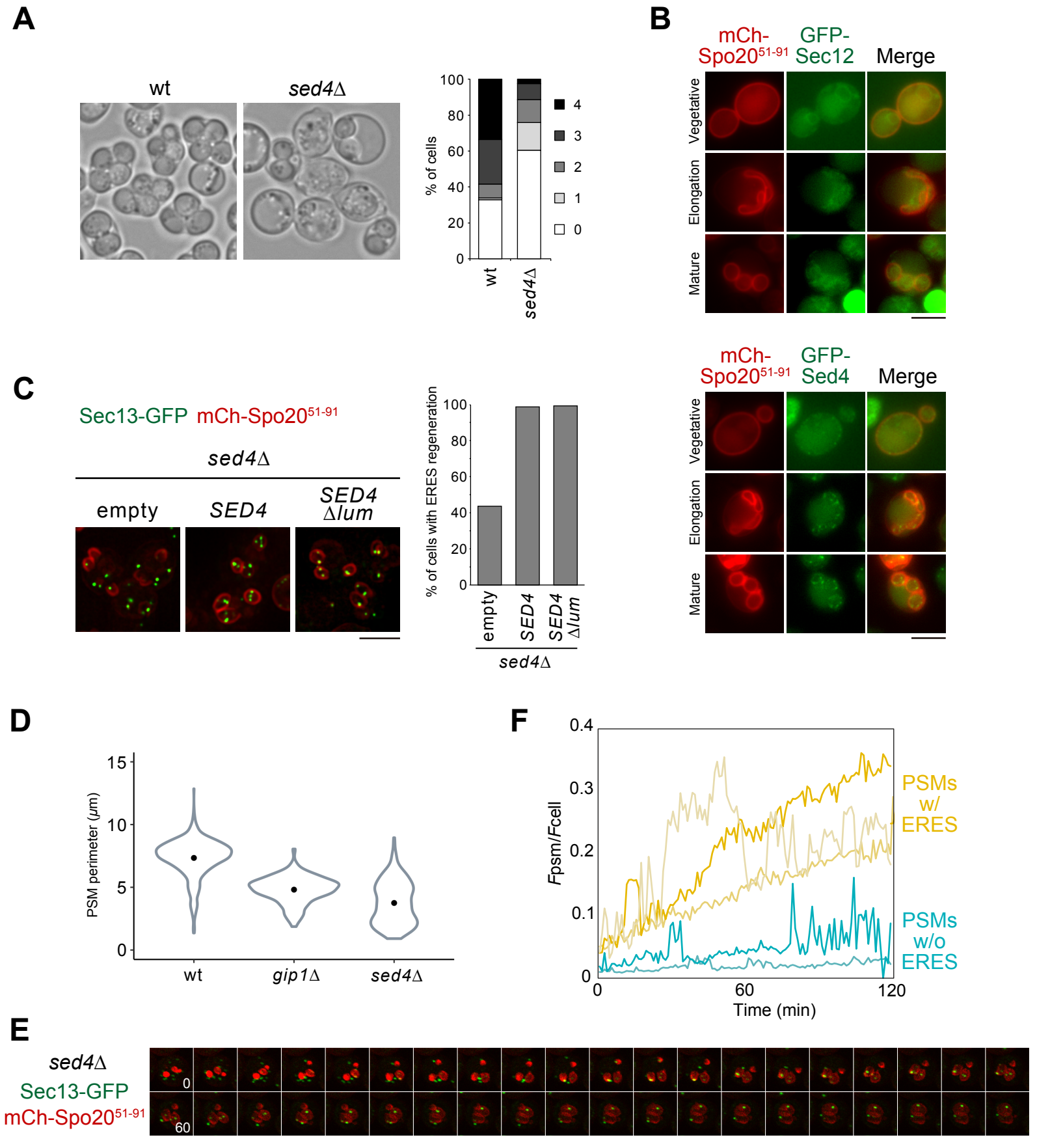
A
wt
sed4Δ
% of cells
100
80
60
40
20
0
4
3
2
1
0
wt
sed4Δ
B
mCh-Spo20^51-91
GFP-Sec12
Merge
Vegetative
Elongation
Mature
C
Sec13-GFP mCh-Spo20^51-91
sed4Δ
empty
SED4
SED4 Δlum
% of cells with ERES regeneration
100
80
60
40
20
0
empty
SED4
SED4 Δlum
sed4Δ
mCh-Spo20^51-91
GFP-Sed4
Merge
Vegetative
Elongation
Mature
D
PSM perimeter (μm)
15
10
5
0
wt
gip1Δ
sed4Δ
F
Fpsm/Fcell
0.4
0.3
0.2
0.1
0
0
60
120
Time (min)
PSMs w/ ERES
PSMs w/o ERES
E
sed4Δ
Sec13-GFP
mCh-Spo20^51-91
0
60

Figure 8

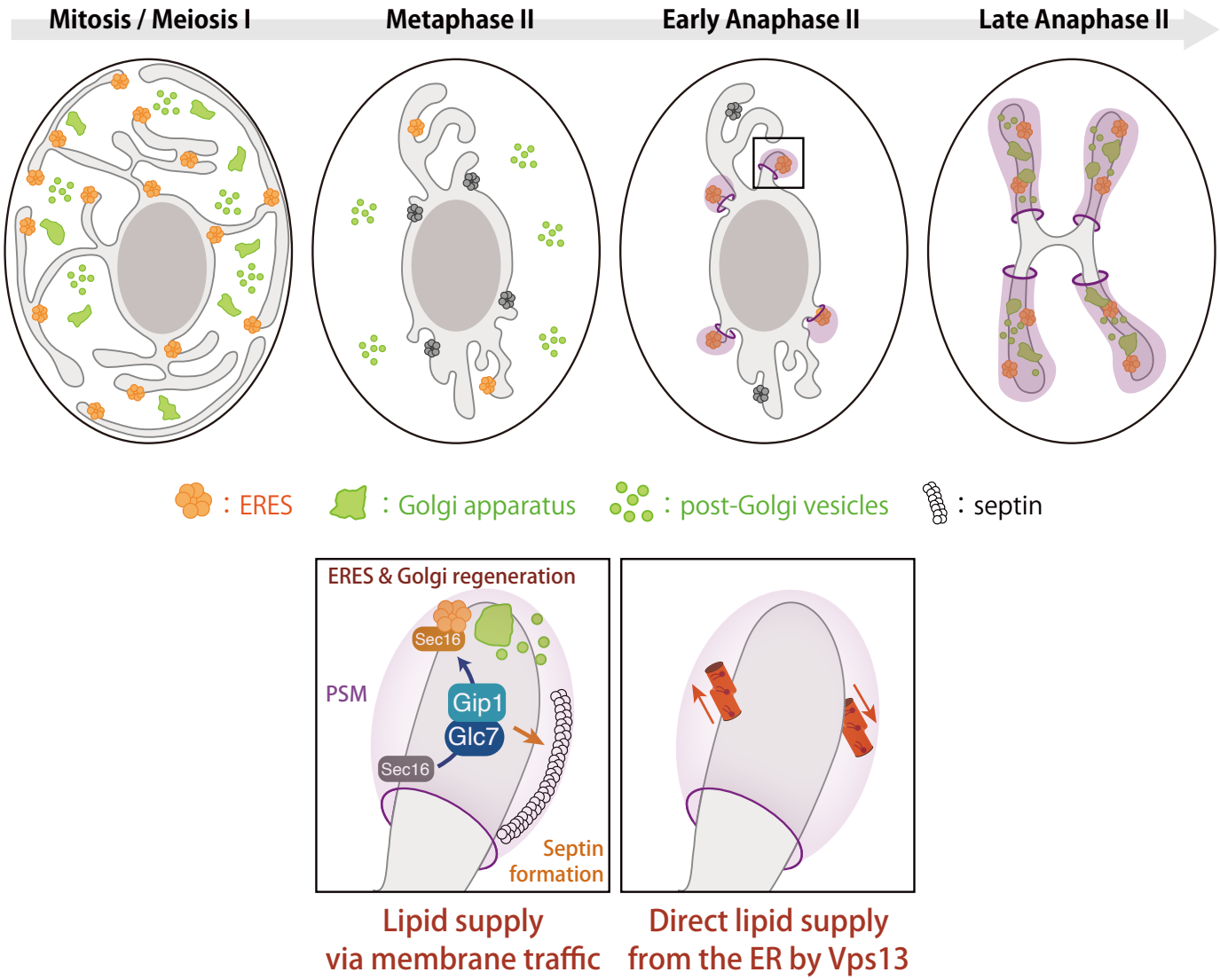
Mitosis / Meiosis I
Metaphase II
Early Anaphase II
Late Anaphase II
: ERES
: Golgi apparatus
: post-Golgi vesicles
: septin
ERES & Golgi regeneration
Sec16
PSM
Gip1
Glc7
Sec16
Septin formation
Lipid supply via membrane traffic
Direct lipid supply from the ER by Vps13

Figure S1

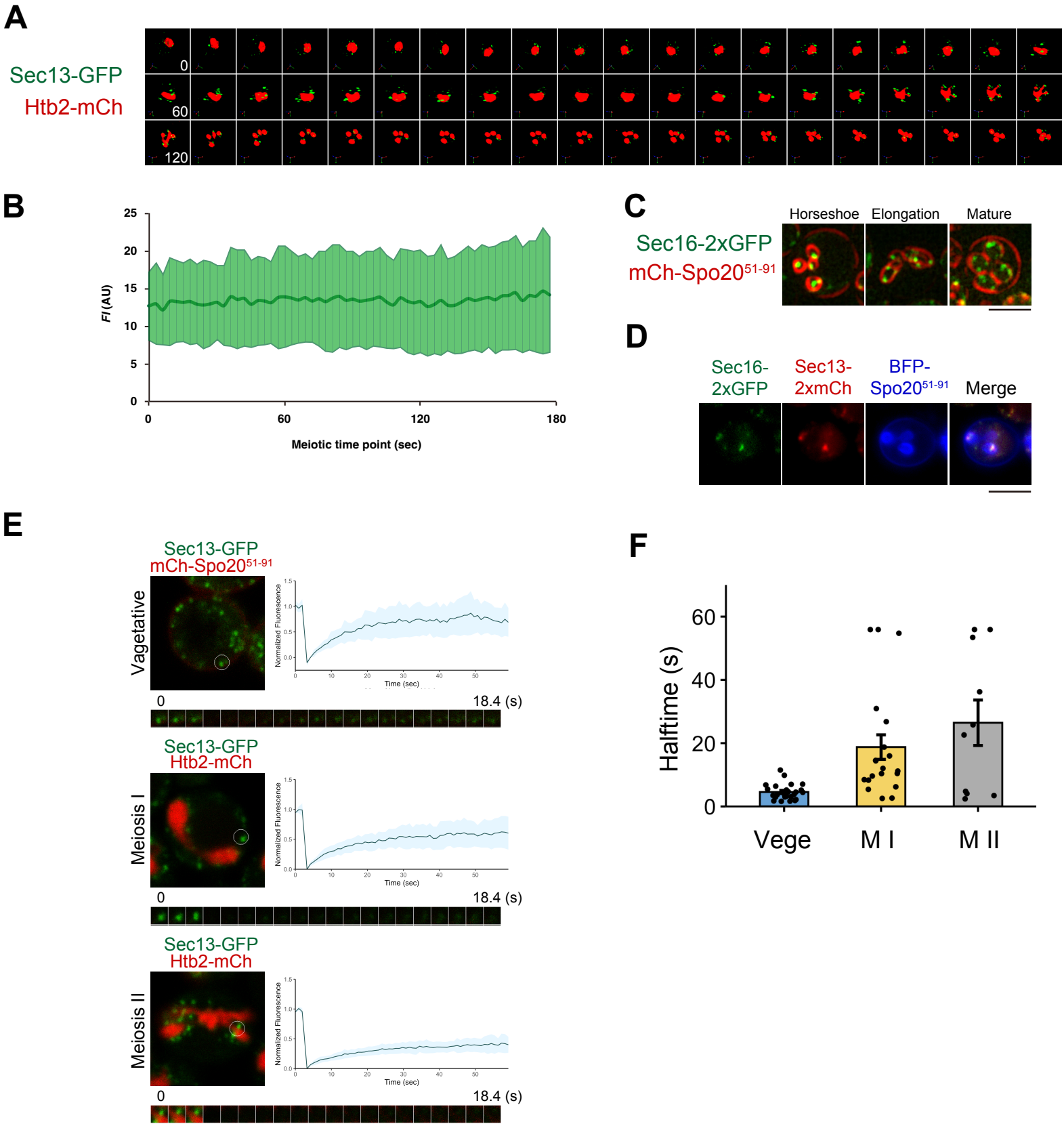
A
Sec13-GFP
Htb2-mCh
0
60
120
B
25
20
15
10
5
0
FI (AU)
0
60
120
180
Meiotic time point (sec)
C
Sec16-2xGFP
mCh-Spo20$^{51-91}$
Horseshoe
Elongation
Mature
D
Sec16-2xGFP
Sec13-2xmCh
BFP-Spo20$^{51-91}$
Merge
E
Sec13-GFP
mCh-Spo20$^{51-91}$
Vagetative
Normalized Fluorescence
Time (sec)
0
18.4 (s)
Sec13-GFP
Htb2-mCh
Meiosis I
Normalized Fluorescence
Time (sec)
0
18.4 (s)
Sec13-GFP
Htb2-mCh
Meiosis II
Normalized Fluorescence
Time (sec)
0
18.4 (s)
F
Halftime (s)
60
40
20
0
Vege
M I
M II

Figure S2

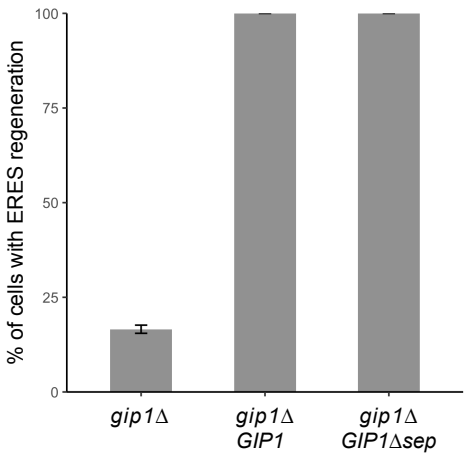
% of cells with ERES regeneration
100
75
50
25
0
gip1Δ
gip1Δ GIP1
gip1Δ GIP1Δsep